

<https://doi.org/10.1038/s41541-025-01160-7>

Hamsters immunized with formalin-inactivated SARS-CoV-2 develop accelerated lung histopathological lesions and Th2-biased response following infection

Check for updates

Rineke de Jong¹ ✉, Sandra Vreman¹, Katrin E. Wiese¹, Nora M. Gerhards¹, Kevin R. Bewley², Yper Hall², Francisco Javier Salguero², Miles Carroll³, Rik L. de Swart¹, Jose L. Gonzales¹ & Nadia Oreshkova¹ ✉

One of the concerns regarding vaccine safety during the COVID-19 pandemic was the potential manifestation of vaccine-associated enhancement of disease (VAED) upon SARS-CoV-2 infection. To investigate the suitability of the Syrian hamster model to test for VAED, we immunized animals with an experimental formaldehyde-inactivated, alum-adjuvanted SARS-CoV-2 vaccine preparation. In two independent experiments, challenge infection did not result in an enhancement of the clinical disease in vaccinated animals compared with mock-vaccinated animals. However, at early timepoints (2–5 days) post-challenge, lung histopathology progressed faster and was more prominent in vaccinated hamsters and lung tissue showed elevated mRNA levels of IL-4 and IL-13. At later time points, cytokine responses and lung pathology were comparable between vaccinated and mock-vaccinated hamsters, underscoring the transient nature of the pathological aggravation. With this work we show that the Syrian hamster model can be used to assess possible vaccine safety considerations in a preclinical setting.

The coronavirus disease 2019 (COVID-19) pandemic led to an unprecedented global effort to develop SARS-CoV-2 vaccines. As a result, a wide range of vaccines were approved worldwide for use in humans during the pandemic. These vaccines include mRNA vaccines, vector vaccines, subunit vaccines and inactivated whole virus vaccines. At the dawn of the vaccine development for SARS-CoV-2, one of the safety concerns was related to manifestation of events of vaccine-associated enhancement of disease (VAED). Up until now, there are no records for such events in individuals that have received any type of vaccine against COVID-19. Nevertheless, it remains important to monitor the phenotype of the immune response and the possible display of VAED in newly developed and in existing vaccines.

VAED can manifest in individuals who have been vaccinated and subsequently contract an infection with the pathogen targeted by the vaccine. It is defined as a disease presenting with more severe symptoms, or disease with modified/unusual clinical manifestation¹. VAED is a well-described

phenomenon in the context of formalin-inactivated whole virus vaccines against human respiratory syncytial virus (HRSV) and measles virus (MeV) used in the 1960s. A formalin-inactivated alum-adjuvanted HRSV vaccine was applied to young children and, upon natural infection, was associated with significantly increased hospitalization rate and two fatalities in the vaccinees as compared with the control group². The disease was characterized by high fever and massive infiltration of immune cells into the lungs, pointing towards an immunopathological mechanism. This hypothesis was further supported by studies in animal models, where challenge infection of vaccinated animals induced severe lung lesions associated with infiltration of granulocytes (e.g. neutrophils and eosinophils) and monocytes/macrophages, Th2-bias of the immune response and the presence of low-avidity, non-protective antibody responses that contributed to accumulation and deposition of immune complexes and complement-mediated injury in lungs (reviewed in refs. 3–6). Similar mechanisms have been described as the cause

¹Wageningen Bioveterinary Research, Wageningen University and Research, Lelystad, The Netherlands. ²United Kingdom Health Security Agency (UKHSA), Porton Down, Salisbury, UK. ³Centre for Human Genetics and the Pandemic Sciences Institute, Nuffield Department of Medicine, University of Oxford, Oxford, UK. ✉ e-mail: rineke.jong@wur.nl; Nadia.oreshkova@wur.nl

for developing “atypical measles” in association with a formalin-inactivated MeV vaccine³⁷. For both HRSV and MeV vaccines, formalin inactivation is suspected to be a contributing factor to the Th2 polarization of the immune response, since carbonyl groups generated during the inactivation process were shown to favor Th2 responses in mice⁸. Furthermore, alum-based adjuvants are recognized for driving Th2 skewing of the immune response^{9,10}, and aluminum hydroxide was used as adjuvant for the formalin-inactivated HRSV vaccine.

With respect to human respiratory coronaviruses, two new coronaviruses had emerged before the pandemic SARS-CoV-2 in 2019, namely SARS-CoV (in 2002–2003) and MERS-CoV (in 2012). For both viruses, diverse vaccines were tested in preclinical models and results that potentially reflect VAED were reported. In the context of SARS-CoV, a formalin-inactivated SARS-CoV vaccine was associated with increased lung lesions after challenge infection in non-human primates¹¹. A double-inactivated (with formalin and ultraviolet irradiation) whole SARS-CoV vaccine, either adjuvanted with alum or not, was poorly protective against disease and viral replication, and induced eosinophilic immunopathology in the lungs of aged mice following either homologous or heterologous challenge infection. Young mice were well protected and did not show lung pathology following homologous challenge but were only partially protected and displayed lung pathology following heterologous challenge¹². Other types of vaccines have also been shown to induce immunopathological lesions in the lungs of mice^{13–15} or non-human primates¹⁶. For MERS-CoV, a gamma-irradiated whole virus vaccine (either adjuvanted with Alum, MF59 or non-adjuvanted) was found to bear risk for hypersensitive-type lung pathology in mice, characterized by lung infiltrates consisting of mononuclear cells and eosinophils, and increased levels of IL-5 and IL-13¹⁷. A similar hypersensitivity-type response was reported in mice vaccinated with UV-inactivated, alum adjuvanted MERS-CoV¹⁸. It should be noted that the pathological results of some of these studies^{11,13,16,17} were discussed controversially by others⁶. However, collectively these studies suggest that VAED can be induced by inactivated coronavirus vaccines in preclinical models, therefore implying that initial safety concerns regarding vaccines developed against SARS-CoV-2 were reasonable.

To support safety assessment of novel vaccines for COVID-19, several animal models were used to test if VAED can be induced after SARS-CoV-2 infection in the context of vaccine-induced immunity. In all studies, vaccine preparations that are expected to induce VAED were used, such as formalin-inactivated whole virus preparations^{19–21}, denatured S protein vaccines²¹ or recombinant spike protein^{22–24}, for all of which except one study²⁰, alum was used as adjuvant. While no VAED was observed in macaques, vaccinated ferrets did show a transient increased pathology compared to mock-vaccinated animals, characterized by eosinophilic infiltrates and perivascular cuffing in the lung observed at 6 to 7 days post infection (DPI), which resolved by 13 to 15 DPI¹⁹. In mice, Th2 skewing as well as eosinophilic and neutrophilic infiltrates in the lungs were found early post infection, at 3 or 4 DPI, while the animals were partially protected from clinical signs and viral replication^{21,22}. At a later time point post infection (7 DPI), murine lungs exhibited severe immunopathology, characterized by significant perivascular infiltration of eosinophils and CD4+ T cells, and increased expression of Th2/Th17 cytokines²⁴. Two studies have been described in golden Syrian hamsters, with opposing findings. In one study, hamsters vaccinated twice with a formalin inactivated vaccine had only limited pulmonary inflammatory infiltrates confined to the alveolar walls at 4 DPI, and had more pronounced Th1 cytokines in lungs as compared with control hamsters (Th2 cytokines were not reported)²⁰. In the other study, an alum-adjuvanted, non-stabilized spike protein vaccine induced VAED represented by pronounced Th2 cytokine production and massive eosinophilic infiltration in lung tissue at 4 DPI²³. In all aforementioned studies, a single necropsy point after challenge was used to evaluate lung pathology.

To investigate the potential occurrence of VAED in Syrian hamsters in the context of a formalin-inactivated whole virus preparation (FIWV) adjuvanted with alum, we performed two experiments. In the first experiment, we sought vaccine conditions that result in VAED. To that end, four

different vaccine regimens comprising two different antigen doses applied in either single or prime-boost administration regimen were used to determine if and under which condition(s) VAED would occur. Based on the outcome of the first experiment, a second experiment was designed to study the kinetics of VAED during the course of infection, using the vaccine regimen that had resulted in the most pronounced VAED in the first experiment. Vaccinated hamsters were compared with mock-vaccinated hamsters and hamsters that had recovered from a previous homologous SARS-CoV-2 challenge (re-challenge group). Our findings reveal an accelerated onset of lung lesions in vaccinated hamsters compared to mock-vaccinated controls. Although the differences were transient, neutralizing antibodies in vaccinated hamsters were absent prior to challenge, and more pronounced Th2 responses were observed in lung tissue early after infection.

Results

FIWV vaccination provides partial clinical protection and no aggravation of clinical signs after SARS-CoV-2 infection

In the first study, four different immunization regimens with formalin-inactivated whole virus (FIWV) SARS-CoV-2 preparations were tested (Fig. 1, upper panel) and one group of hamsters served as mock-vaccinated control (mock-vaccinated group). Following challenge infection, all groups exhibited loss of body weight (Fig. 2a), which in the mock-vaccinated group was most pronounced between 5 and 7 DPI. Only the 2x high dose vaccine regimen showed significant reduction of body weight loss compared with the mock-vaccinated group (Fig. 2b). The hamsters of the 1x high dose group also trended towards a reduction in body weight loss, albeit not significantly (Fig. 2a, b). There was a reduction in activity post SARS-CoV-2 inoculation in all groups, starting from 2 DPI (Fig. 2c, d). From 6 DPI onwards, activity increased and pre-inoculation activity levels were reached on 10 DPI. No statistically significant differences between the groups were found (Fig. 2d). Overall, no aggravation of clinical signs was observed in the vaccinated groups compared with the mock-vaccinated group.

FIWV vaccination fails to induce neutralizing antibodies prior to challenge and does not protect from virus replication in the lungs after challenge

Viral loads in lung tissue samples were assessed by subgenomic (sg)RNA PCR, which is indicative for virus replication²⁵. High viral loads were detected in lung tissue of hamsters from the mock-vaccinated group on 5 DPI (9.32 log₁₀ RNA copies per gram tissue on average) (Fig. 2e). The vaccinated groups trended towards slightly decreased RNA loads, most obvious in the group vaccinated with the 2x high dose (Supplementary Table S1). Differences between the treatment groups and the mock-vaccinated group were not significant. On 13 DPI, no sgRNA was detected anymore.

Neutralizing antibodies were not detected in any of the pre-challenge sera (-2/-1 DPI), except in two samples with low titers (5.7 and 10) in the group vaccinated with 2x high dose regimen. All groups had measurable neutralizing titers post challenge and interestingly, no significant differences were observed between vaccinated and mock-vaccinated hamsters at 5 DPI (Fig. 2f and Supplementary Table S2). These results indicate that neither of the vaccination regimens provided sufficient priming of a neutralizing antibody response. Two of the groups, 1x high dose and 1x low dose, showed significant increase in titers between 5 and 13 DPI, and the 1x low dose group was the only one with higher titers than the mock-vaccinated animals at 13 DPI, indicating overall different kinetics in humoral response between the groups that had received different vaccination regimens.

FIWV vaccination transiently aggravates lung pathology in hamsters

On -1, 5 and 13 DPI, four animals each per group were sacrificed and SARS-CoV-2-related lung lesions were evaluated. Relative lung weights of hamsters from all groups were comparable on -1 DPI. Hamsters in all treatment groups showed a significant increase in relative lung weight at 5 DPI, reflecting the presence of inflammatory responses in the lung (Fig. 3a,

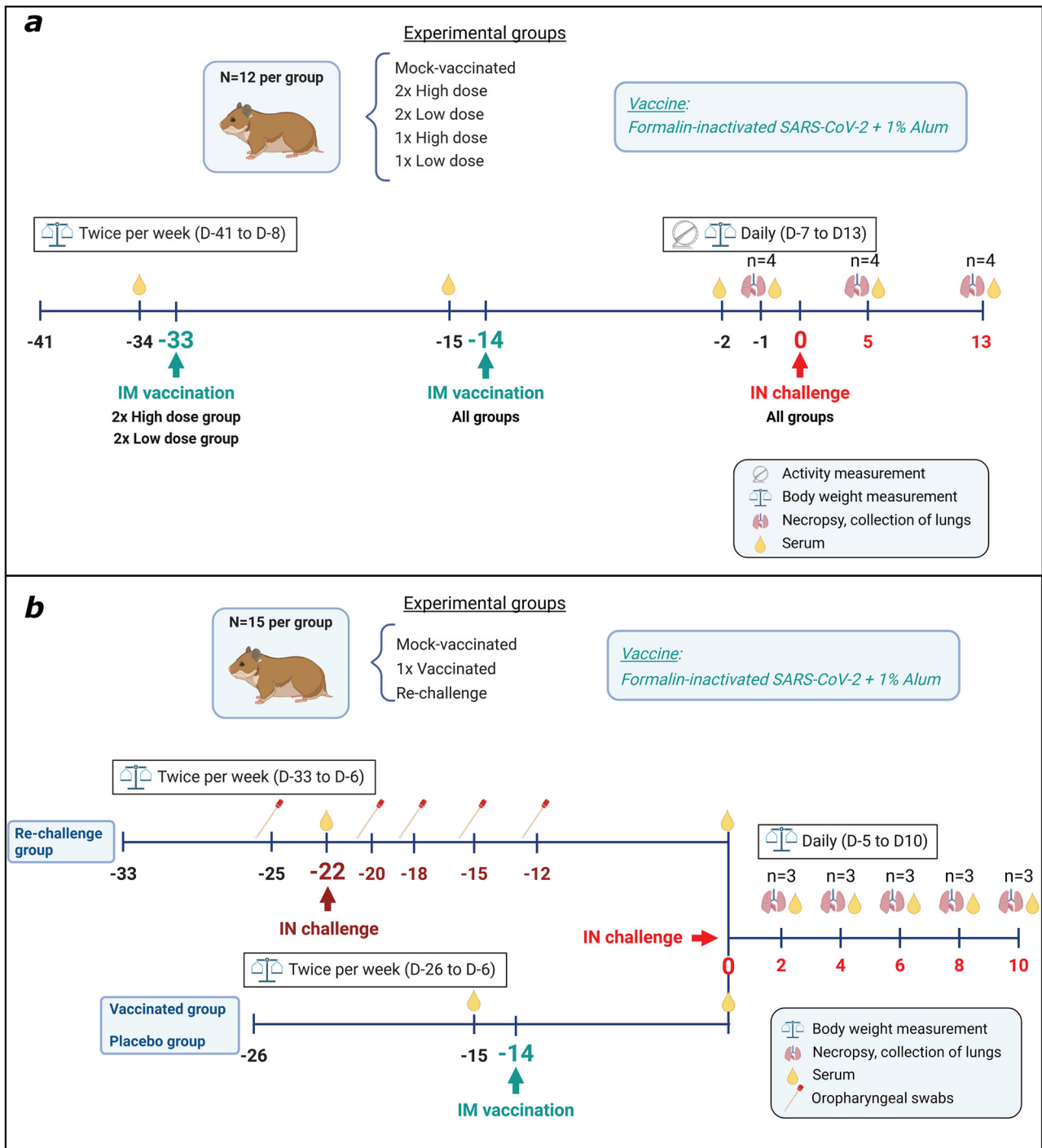


Fig. 1 | Schematic representation of study designs for. a VAED model development: establishing vaccination conditions that result in VAED and **b** VAED kinetics: studying the kinetics of VAED during infection. Timelines for both studies are

shown, with the respective handlings and measurements. Numbers in black: acclimatization days; numbers in green: days of vaccination; numbers in brown/red—days post challenge infection. Illustrations were created with biorender.com.

significance annotation not shown). At 13 DPI lung weights had decreased again without reaching baseline levels. The decrease was significant only in the 1x high dose group, suggestive of an inflammation process that is more acute and/or with different dynamics in this group. There were no significant differences in relative lung weights between any of the treatment groups and the mock-vaccinated group on either time point post challenge infection (5 or 13 DPI). However, lungs of most vaccinated hamsters trended towards a higher relative weight compared with the mock-vaccinated group on 5 DPI. This trend was most pronounced in the 1x high dose vaccinated group.

No histopathological lesions were observed in any of the lungs before challenge infection (Fig. 3b, c, -1 DPI). On 5 DPI, lungs of hamsters of all groups showed clear SARS-CoV-2-related histopathologic changes. Interestingly, the extent of lung lesions was the least prominent in animals from the mock-vaccinated group, as compared with the vaccinated animals (Fig. 3d, e and Supplementary Table S3). The differences between the mock-vaccinated group and the two groups that had received single dose vaccinations were significant (Fig. 3b). These results were confirmed in an independent evaluation performed by a second pathologist (Supplementary Fig. S1, $R^2 = 0.94$). Severity of histopathological changes was graded based on six different

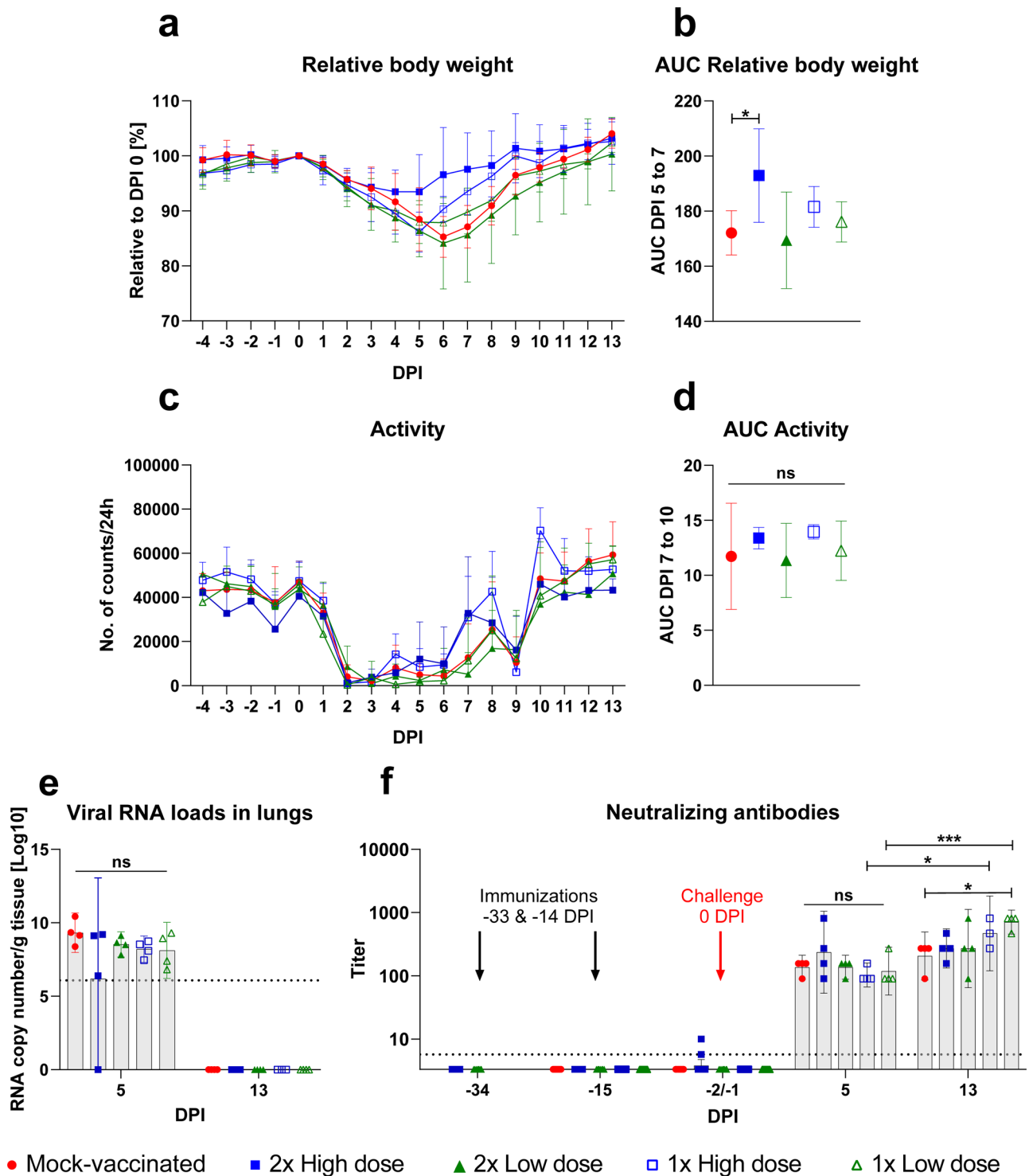


Fig. 2 | VAED model development study: relative body weight, activity, viral loads and neutralizing antibody responses in hamsters after different regimens of FIWV vaccination and SARS-CoV-2 challenge infection. a Relative body weight over time expressed as percentage of body weight on the day of challenge (0 DPI) ($n = 8$ per group up to 5 DPI and $n = 4$ between 6 DPI and 13 DPI; $n = 7$ and $n = 3$ respectively for group 1x high dose). **b** Mean area under the curve (AUC) per group for the period when the mock-vaccinated group had the lowest body weight, 5 to 7 DPI. Hamsters sacrificed on 13 DPI were used for the calculation ($n = 4$ or $n = 3$ for group 1x high dose). Only significant differences are indicated. **c** Hamster activity over time, expressed as running wheel rotation counts ($n = 4$ ($n = 3$ for group 1x high dose)). **d** AUC (log-transformed counts) of the 4 days encompassing the period of activity recovery (7–10 DPI), calculated for each hamster. Calculations and data

display were performed on log-transformed counts. **e** Viral RNA loads in lungs, as measured by RT-qPCR detecting subgenomic viral RNA. The 50% limit of detection of the PCR assay is indicated by the dotted line. **f** Neutralizing antibody titers per treatment group displayed over time; $n = 12$ for study days -34, -15 and -2/-1; $n = 4$ ($n = 3$ for group 1x high dose) for 5 and 13 DPI. The dotted line represents the detection limit of the test. Only statistically significant differences are indicated. **a–d** Symbols show group means. **e, f** Symbols show individual values and bars illustrate group means. Error bars in plots a and c show SD (standard deviation), and in all other plots 95% CI (confidence intervals). Differences with p values < 0.05 were considered significant. Level of significance is illustrated with asterisks for the following p values: 0.01 to 0.05 - *; 0.001 to 0.01 - **; 0.0001 to 0.001 - ***; <0.0001 - ****; ns not significant (≥ 0.05). DPI days post infection.

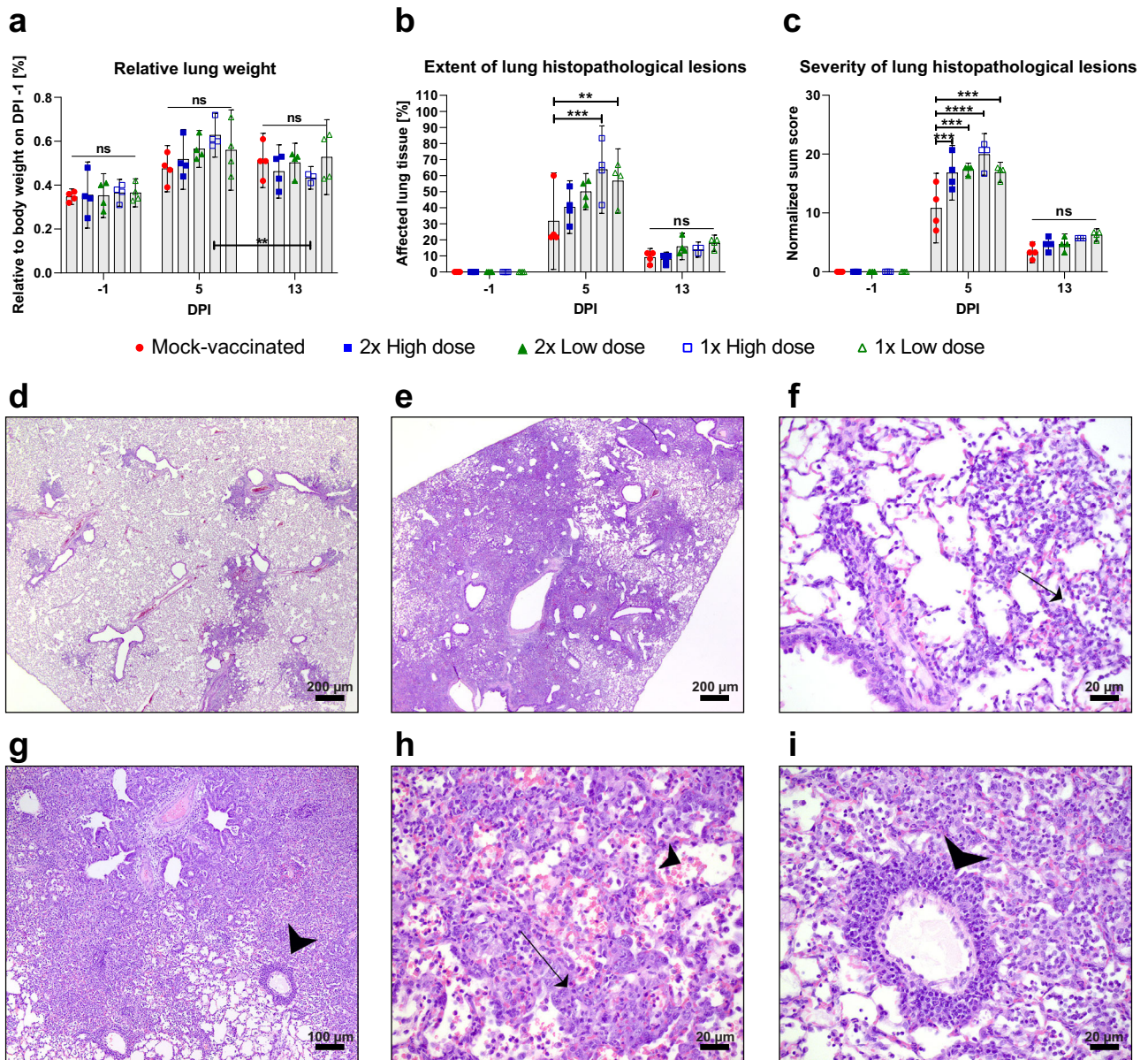


Fig. 3 | VAED model development study: lung (histo)pathology. **a** Relative lung weight of the left lung lobe, expressed as percentage of the body weight determined on -1 DPI. Within-group changes between -1 and 5 DPI were significant (not annotated). **b** Extent of histopathological lesions, expressed as percentage of the total lung area of a section of the whole left lung lobe. Three scorings were performed of each slice and the average values were calculated per hamster and the average values were calculated per hamster per time point. To account for the different scale of the scores, all scores were normalized before calculating the sum. **a–c** Symbols show individual values and bars illustrate group means, $n = 4$ per group except for group 1x high dose on 13 DPI, where $n = 3$. Error bars: 95% CI. Significant differences between groups are illustrated with

asterisks for the following p values: 0.01 to 0.05 - *; 0.001 to 0.01 - **; 0.0001 to 0.001 - ***; <0.0001 - ****; ns not significant (≥ 0.05). DPI days post challenge infection.

d Mock-vaccinated group with mild extent of lung pathology (grade 1–2), often centered around bronchioles; **e** 1x high dose vaccinated group with extensive and coalescing lung histopathology (grade 3); **f** Mock-vaccinated group: alveolar lumina containing macrophages and granulocytes (arrow); **g** 1x high dose group: coalescing lung changes with prominent perivascular infiltrates (arrowhead); **h** 1x high dose group: extensive type II pneumocyte proliferation (arrow) with alveolar hemorrhage (arrowhead); **i** 1x high dose group: perivascular infiltrates with more than 5 layers of cells (arrowhead), grade 3 blood vessel change; **d–i** Representative images from 5 DPI.

parameters (see materials and methods). Overall, histopathological changes were present in all vaccination groups (Supplementary Fig. S2), but the cumulative (“sum”) severity score was the highest in the 1x high dose group (grade 3) compared with the mock-vaccinated group (grade 1 or 2) at 5 DPI (Fig. 3c). The main lesions in mock-vaccinated animals included mild to moderate thickening of alveolar walls, hemorrhages and alveolar infiltrates consisting of macrophages, granulocytes and to a lesser extent of lymphocytes (Fig. 3f). These changes were often centered around the bronchiole. The lungs of vaccinated animals showed more extensive and coalescing changes (Fig. 3e, g), characterized by severe type II pneumocyte proliferation (bulging cells

with plump nuclei) (Fig. 3h), prominent alveolar infiltrates of granulocytes, macrophages and to a lesser extent lymphocytes and plasma cells. Prominent hemorrhages (Fig. 3h) and perivascular infiltrates up to 5 rows were also present (Fig. 3i). The perivascular cuffs were mainly composed of mononuclear cells with fewer interspersed granulocytes. On 13 DPI, most histopathological changes were resolved and there was only a mild type II pneumocyte hyperplasia with minimal perivascular infiltrates. Although there was no statistically significant difference between the mock-vaccinated and the vaccination groups, there was a trend towards slightly higher histopathological changes still present in the vaccinated groups (Fig. 3b, c).

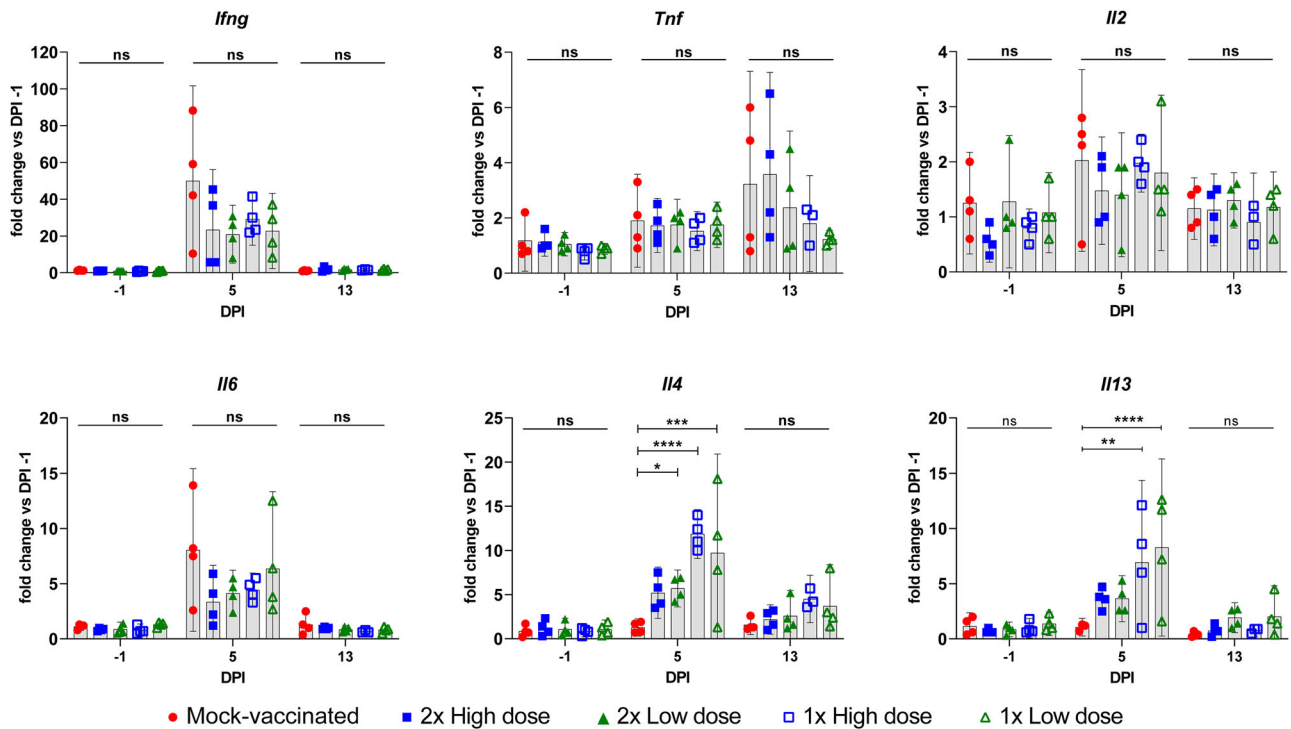


Fig. 4 | VAED model development study: cytokine gene expression in lung tissue as quantified with RT-qPCR. Quantities are expressed as fold change increase compared to baseline levels (in lungs harvested at -1 DPI). Symbols show individual values and bars illustrate group means, $n = 4$ per group except for group 1x high dose on 13 DPI

where $n = 3$. Error bars: 95% CI. Significant differences between groups are illustrated with asterisks for the following p values: 0.01 to 0.05 - *; 0.001 to 0.01 - **; 0.0001 to 0.001 - ***; <0.0001 - ****; ns not significant (≥ 0.05). DPI days post challenge infection.

Evaluation for virus infection of lung tissue with immunohistochemistry (IHC) staining revealed viral nucleoprotein (N) expression in nearly all animals on 5 DPI, with a variable extent from grade 1 to grade 3 (Supplementary Fig. S3a). N-protein expression was mainly found in pneumocytes and alveolar macrophages and to a lesser extent in bronchi and bronchiole (Supplementary Fig. S3d, e). There were no significant differences between mock-vaccinated and vaccination groups and no correlation between the presence of viral antigen and the extent (Supplementary Fig. S3b) or severity (Supplementary Fig. S3c) of histological lesions. No nucleoprotein expression was detected by IHC on 13 DPI.

FIWV vaccination promotes a Th2-skewed cytokine profile in the lung

Expression of key Th1 and Th2 cytokines in lung tissue was quantified by RT-qPCR (Fig. 4). *Ifng*, *Il6* and *Il2* expression was elevated in all groups at 5 DPI and returned to (nearly) baseline levels at 13 DPI, while an increasing trend was observed for *Tnf* over time. No significant differences among the groups were observed for any of these classical Th1 cytokines at any time point. Expression of Th2-type cytokines *Il4* and *Il13*, however, was markedly increased in all vaccination groups at 5 DPI, with significant differences in the groups 2x low dose (only *Il4*), 1x high dose and 1x low dose compared with the mock-vaccinated animals. At 13 DPI, *Il4* and *Il13* mRNA levels returned to near baseline levels with no significant differences between groups.

Collectively, the 1x high dose FIWV group showed the most pronounced lung histopathology at 5 DPI, as well as significant upregulation of Th2-associated cytokines. Therefore, this vaccination regimen was selected for a follow-up experiment, in which the kinetics of pathology and expression of genes associated with Th-type immune biases were evaluated in more detail.

Single, high-dose FIWV vaccination provides partial protection against SARS-CoV-2 infection-associated body weight loss

One group of hamsters ($n = 15$) was vaccinated once with high dose of FIWV. Two groups served as controls: one was vaccinated with PBS (mock),

and another one was challenged with SARS-CoV-2 D614G 3 weeks prior to challenge infection of all three groups with the same virus strain (re-challenge group) (Fig. 1, lower panel). The first infection of the re-challenge group was confirmed by analyzing viral loads in oropharyngeal swabs (Supplementary Fig. S4a). Post challenge, the highest relative body weight loss in the mock-vaccinated group was observed between 5 and 7 DPI (Fig. 5a) and maximum weight loss (average of 15.9%) was comparable to the first study (average of 14.9%). The re-challenged control animals were protected from body weight loss. The vaccinated hamsters in this study lost significantly less body weight compared to mock-vaccinated animals, but significantly more than the fully protected re-challenged hamsters (Fig. 5b).

FIWV vaccination reduces duration of viral replication in the lung after challenge, but does not prime neutralizing antibody response

Subgenomic RNA (sgRNA) in lung samples was not detectable in the re-challenged animals, indicating lack of active virus replication (Fig. 5c). The vaccinated animals were positive for sgRNA in lungs collected on 2 and 4 DPI. From 6 DPI onwards, sgRNA was not detectable in the vaccinated animals any longer, while sgRNA was detected in all tested mock-vaccinated animals up to 8 DPI. To confirm that virus reached the lungs in the re-challenge group upon the second infection, we also performed PCR for total viral E gene RNA. Re-challenged animals had relatively constant amounts of RNA in the lungs for the whole post-challenge observation period, indicative of lack of virus replication (Supplementary Fig. S4b and Table S4). Detected viral RNA was most likely the result of virus inoculum that had been taken up by immune cells to facilitate clearance. In contrast, both the mock-vaccinated and the vaccinated groups had higher levels of total viral RNA at 2 DPI, which then gradually decreased over time. By 10 DPI, total viral RNA levels were comparable to those in the re-challenged group.

No neutralizing antibodies (NA) were detected in vaccinated animals prior to challenge (Fig. 5d), corroborating previous results with the same vaccination regimen (Fig. 2f). After challenge infection, only one out of three

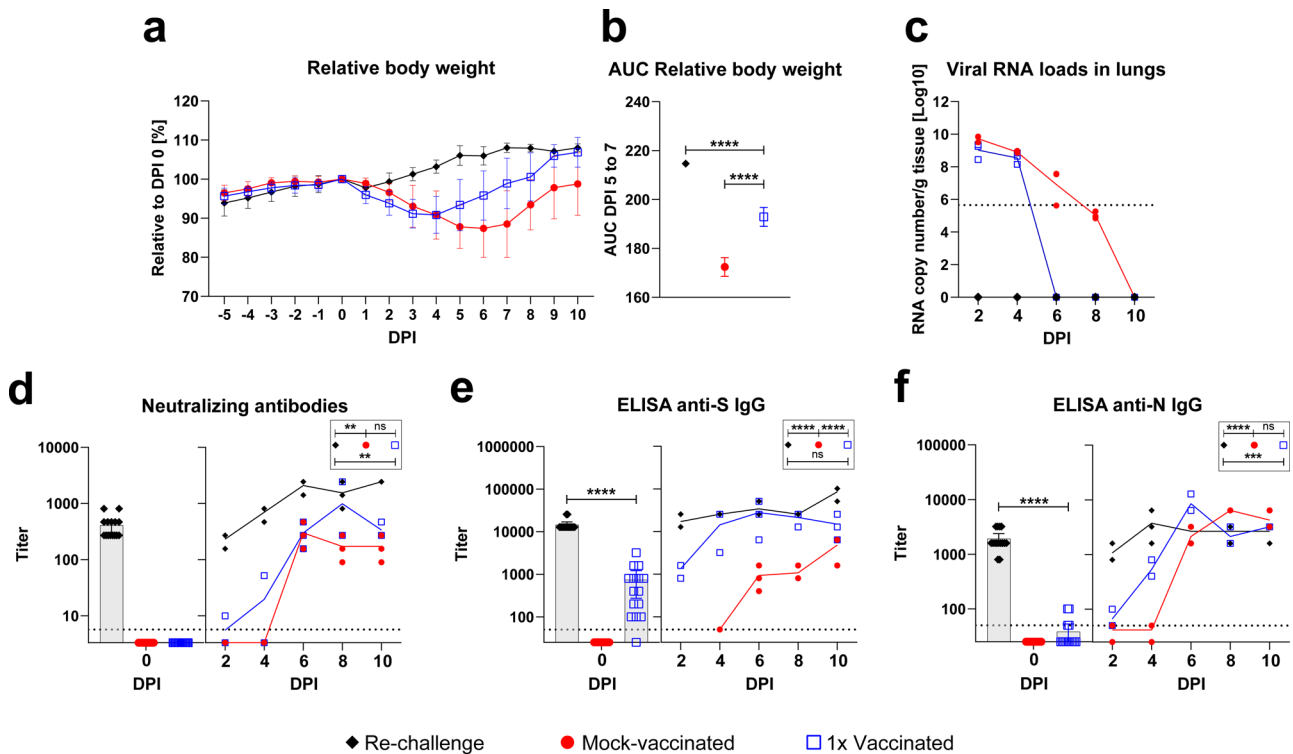


Fig. 5 | VAED kinetic study: relative body weight, viral loads and antibody responses following challenge infection with SARS-CoV-2. **a** Relative body weight over time expressed as percentage of body weight on the day of challenge infection (0 DPI); $n = 15$ at 0 DPI and decreasing with 3 hamsters on every even DPI. **b** Area under the curve (AUC) for 5 to 7 DPI, calculated for each hamster and shown as group means ($n = 6$, subgroups sacrificed at 8 and 10 DPI were used for graphical representation and statistical analysis). Only significant differences are indicated. **c** Viral RNA loads in lung tissue, as measured by RT-qPCR detecting subgenomic viral RNA. The 50% limit of detection of the PCR assay is indicated by the dotted line. No viral RNA was detected in the re-challenged animals. **d** Neutralizing antibody titers (end-point titers). Left panel shows datapoints at 0 DPI ($n = 15$). Right panel displays titers post challenge over time

($n = 3$ per time point). End-point ELISA titers of total anti-spike (**e**) and anti-nucleoprotein (N) (**f**) IgG antibodies. Left panels show datapoints at 0 DPI ($n = 15$). Right panels display titers post challenge over time ($n = 3$ per time point). The dotted lines in all plots represent the detection limit of the respective test. **a, b** Symbols show group means; **c-f** Symbols show individual values, $n = 3$ per group per timepoint; **d-f** bars illustrate group means. Error bars in plot **a** shows SD, and in all other plots 95% CI. Differences in group means (**b**) and group contrasts over time between 2 and 6 DPI (**d-e**) with p values < 0.05 were considered significant. Level of significance is illustrated with asterisks for the following p values: 0.01 to 0.05 - *; 0.001 to 0.01 - **; 0.0001 to 0.001 - ***; < 0.0001 - ****. DPI days post challenge infection.

vaccinated animals had detectable NAs at 2 DPI and one out of three at 4 DPI. From 6 DPI onwards, all vaccinated and all mock-vaccinated animals were NAs positive. The overall kinetics of the NA response in vaccinated hamsters was similar to what was observed for hamsters in the mock-vaccinated group, and significantly different from the re-challenged group. All re-challenged animals had NAs already at 0 DPI, three weeks after the first virus inoculation and titers increased further following re-challenge. In contrast to the NAs, spike-binding IgG antibodies were found in all but one vaccinated hamster (Fig. 5e) at 0 DPI, although titers were significantly lower and more variable than the titers in the re-challenged group. However, the overall kinetics of the anti-spike (S) binding antibodies of the vaccinated hamsters was similar to the re-challenged hamsters and significantly different from the kinetics in the naïve hamsters from the mock-vaccinated group. Anti-nucleoprotein (N) antibodies were found in 3 out of 15 vaccinated hamsters prior to challenge (Fig. 5f). Titers of these antibodies increased earlier than in the hamsters of the mock-vaccinated group but followed the same kinetics. The re-challenged group had the highest anti-N titers early after infection and the titers remained stable over time.

Single, high-dose FIWV vaccination accelerates lung pathology characterized by prominent perivascular infiltrates

To evaluate kinetics of lung pathology in more detail over time, necropsies were performed at 2, 4, 6, 8 and 10 DPI. On both macroscopic level (based on relative lung weights, Fig. 6a) and on histological level (based on extent and severity of pathological lesions, Fig. 6b, c), pathological lesions occurred with accelerated kinetics in the vaccinated group as compared with the

mock-vaccinated group. The scores of all evaluated histopathological parameters increased earlier in the vaccinated group (between 2 and 6 DPI) (Fig. 6a-d and Supplementary Fig. S5), consistent with the differences observed at 5 DPI in the model development study. Notably, SARS-CoV-2-related pathological lung changes in the mock-vaccinated group reached a similar magnitude as in the vaccinated group, but at a later timepoint (at 8 DPI), when the lung pathological lesions in the vaccinated group already started to resolve. However, two observations revealed more prominent lesions in the vaccinated, as compared with the mock-vaccinated hamsters. First, on the macroscopic level, the peak in relative lung weight in the mock-vaccinated animals was observed at 6 DPI but overall remained lower than in the vaccinated group (Fig. 6a), suggestive of higher inflammation burden in the lungs of the vaccinated hamsters. Second, on the histological level, the perivascular cuffing up to 6 DPI was consistently more pronounced in the vaccinated animals as compared to the mock-vaccinated animals and from 8 DPI decreased in both groups (Fig. 6d, g, h and Supplementary Fig. S5). Perivascular infiltrates were composed of mononuclear cells intermingled with granulocytic cells (eosinophilic, heterophilic or neutrophilic) (Fig. 6i). In the re-challenged group, hamsters displayed only mild histopathological changes characterized by a mild increase of inflammatory cells within the alveoli (throughout the whole observation period), mild thickening of the alveolar walls (between 4 and 10 DPI) and small perivascular infiltrates (observed only on 2 DPI) (Fig. 6j and Supplementary Fig. S5). No other histopathological lesions were observed in this group.

Viral protein expression in the lungs of vaccinated animals clearly trended towards reduced expression over time as compared with the mock-

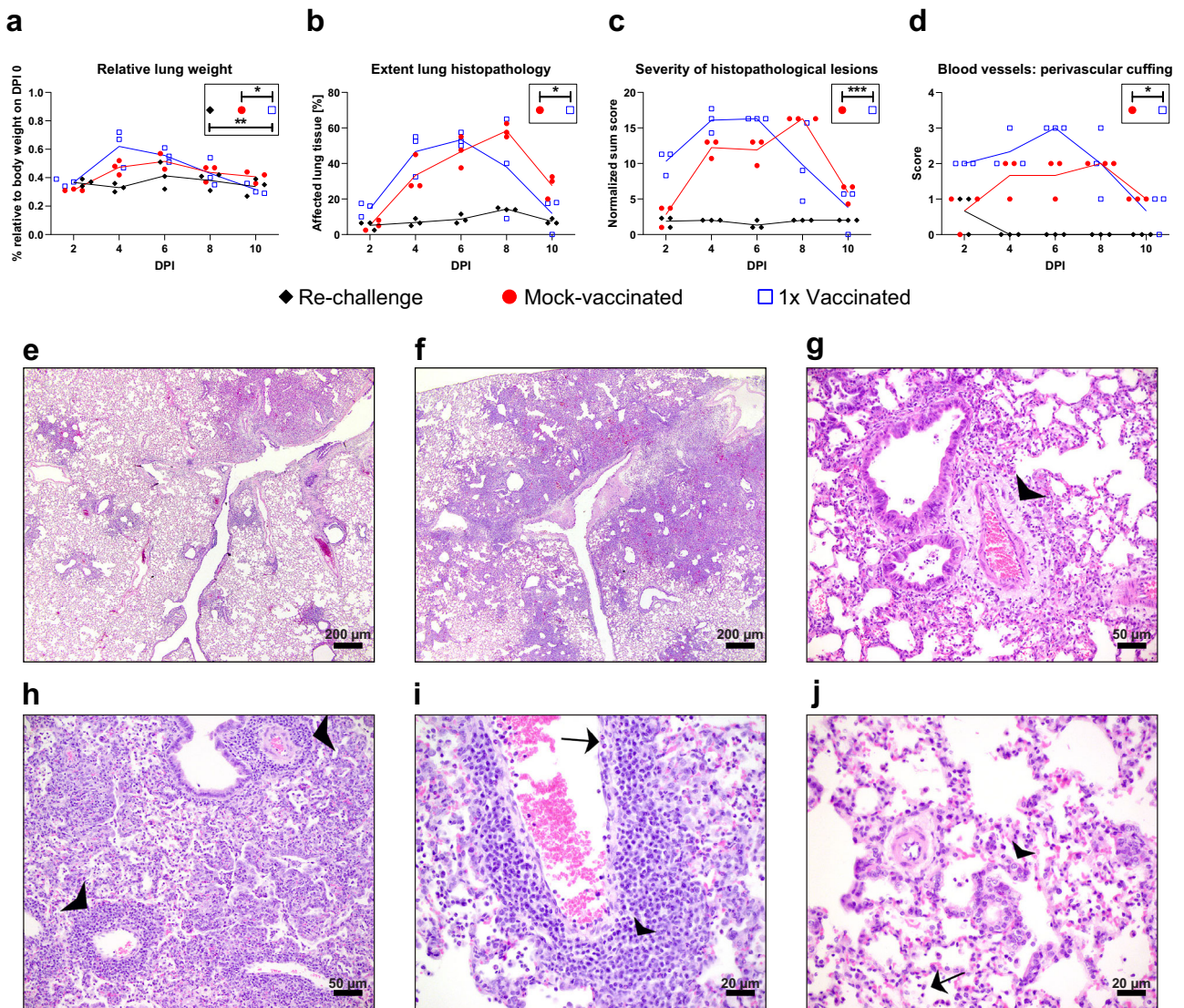


Fig. 6 | VAED kinetic study: evaluation of lung histopathology. **a** Relative lung weight of the left lung lobe, expressed as percentage of the body weight determined at 0 DPI. **b** Extent of histopathological lesions, expressed as percentage of the total lung area of a slice of the left lung lobe. Two scorings were performed of each slice and the average values were calculated per hamster. **c** Severity of histopathological lesions, expressed as cumulative (sum) score of 6 different parameters per hamster per time point. Each of the parameters was scored separately. To account for the different scale of the scores, all scores were normalized before calculating the sum. **d** Severity score for perivascular cuffing of the blood vessels. **a–d** Symbols show individual values and lines represent the group means; $n = 3$ per group per timepoint except for **a** 6 DPI for the mock-vaccinated group (weight of one lung is missing). **e–j** Representative lung histopathology images

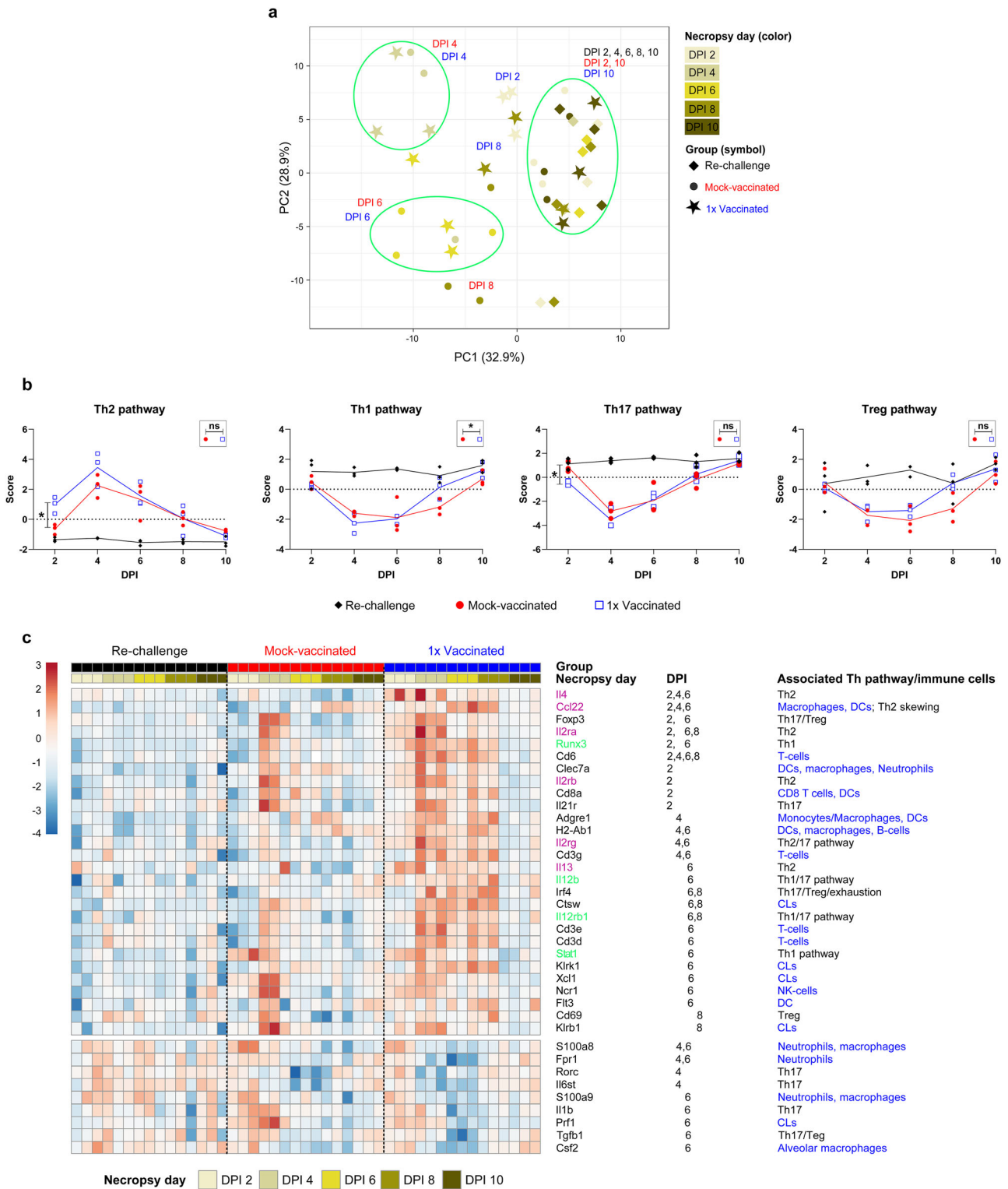
(H&E stain). **e** Lower extent of lung pathology in mock-vaccinated group (4 DPI) compared to **f** Vaccinated group. **g** Mild perivascular infiltrates with edema (arrowhead) in mock-vaccinated group (6 DPI) compared to **h** extensive perivascular infiltrates (arrowheads) in the vaccinated group. **i** Vaccinated group (8 DPI)—extensive infiltrate around large blood vessel composed of lymphocytes, plasma cells (arrowhead) admixed with granulocytes (arrow) and macrophages. **j** Mild histopathologic changes in re-challenge group at 8 DPI, composed of thickening alveolar walls (arrowhead) and infiltrates in alveolar lumina (arrow). Level of significance between group means in time in a–d is illustrated with asterisks for the following p values: 0.01 to 0.05 - *; 0.001 to 0.01 - **; 0.0001 to 0.001 - ***; <0.0001 - ****. DPI days post challenge infection.

vaccinated animals (Supplementary Fig. S6a). No viral protein expression was detected in any of the lungs of the re-challenged animals. The immunohistochemistry scores (used to evaluate the spread of virus in lungs) and the levels of viral sgRNA correlated well in both vaccinated and mock-vaccinated groups (Supplementary Fig. S6b). No correlation was observed between viral protein expression in lungs and extent or severity of histopathological lesions (Supplementary Fig. S6c, d).

Single, high-dose FIWV vaccination promotes a Th2-type cytokine signature in the lung after SARS-CoV-2 infection

A multiplex mRNA analysis of the local immune response to SARS-CoV-2 infection in hamster lungs was performed on $n = 128$ selected genes that are associated with Th1, Th2, Th17 and Treg pathways, and with several

immune cell populations (Supplementary Table S5). Consistent with the clinical and pathological observations, gene expression in the lungs of the vaccinated hamsters was more comparable to the mock-vaccinated hamsters and distinct from the re-challenged animals (Supplementary Fig. S7). Principle component analysis (PCA) revealed that most samples of the re-challenge group clustered relatively closely together regardless of the necropsy day (Fig. 7a), suggesting limited consistent changes in gene expression of the surveyed transcripts over time in response to the second SARS-CoV-2 infection in this group. Based on the first PC, samples of the vaccinated group from 2 DPI separated more clearly from the bulk of both mock-vaccinated and re-challenged animals from the same DPI, which points towards an earlier (“faster”) vaccine-dependent response on gene expression level in the immunized animals. Samples from 4 and 6 DPI



largely formed separate clusters but did not segregate into distinct clusters for the vaccinated and mock-vaccinated groups. Samples obtained on 8 DPI were most variable and spread most heterogeneously. Samples taken on 10 DPI clustered closely with the re-challenge group, suggesting that gene expression changes in response to infection were already attenuated at this point.

Pathway analysis revealed that the Th1, Th2, Th17 and Treg pathways were regulated differently in the mock-vaccinated and the vaccinated groups as compared with the re-challenge group (Fig. 7b). Notably, they followed a

similar trend over time: Th1, Th17 and Treg pathways were downregulated, while the Th2 pathway was up-regulated in both groups. Th2 pathway upregulation followed similar kinetics over time in both groups. However, the magnitude of activation was significantly higher in the vaccinated group at 2 DPI, and still higher (without reaching significance) at 4 DPI (Fig. 7b). Expression levels of individual genes corroborated the pathway scores, since transcripts associated with Th2-skewing of the immune response were upregulated in the vaccinated group, especially early after infection (2 and 4 DPI) (Fig. 7c). There was a marked upregulation of the Th2-associated

Fig. 7 | VAED kinetic study: expression of selected genes and Th-2 skewing in lungs of infected hamsters. Digital nCounter technology was used to survey expression patterns of $n = 128$ genes associated with either Th1, Th2, Th17 and Treg pathways or with different immune cells populations. **a** Principal component analysis based on $\ln(x)$ -transformed normalized count values obtained for all profiled genes in hamster lungs. Unit variance scaling was applied to rows and singular value decomposition with imputation was used to calculate principal components 1 (PC1) and 2 (PC2), which are plotted on the X and Y axis and explain 32.9% and 28.9% of the variance in the dataset, respectively. Colors indicate the different necropsy days and symbols represent different treatment groups. The ellipses in green are only for visualization purposes. **b** Immune response patterns on Th-pathway level. Pathway scores related to the indicated 4 different T cell subsets were plotted over time. Symbols represent individual scores, and the lines shows the group means; $n = 3$ per group per timepoint. Level of significance is illustrated with asterisks for the

following p values: 0.01 to 0.05 - *, 0.001 to 0.01 - **, 0.0001 to 0.001 - ***, <0.0001 - ****. DPI days post challenge infection. **c** Differentially expressed genes on at least one of the necropsy days ($p < 0.05$; no fold change cut-off; $n = 3$ per group and DPI) when comparing vaccinated vs. mock-vaccinated AND vaccinated vs. re-challenge groups. $n = 37$ genes fulfilled these criteria: $n = 28$ were upregulated (upper cluster) and $n = 9$ were downregulated (lower cluster) in association with the vaccination. For any given gene, brown indicates higher expression relative to all samples' average and blue indicates lower expression (difference of $\pm 1 =$ values are one SD away from the average of the row). Note that expression levels can only be compared within a row (i.e. per gene across samples), not between different rows. The numbers in column "DPI" indicate the day(s), when a specific gene was significantly upregulated, as compared to both the mock-vaccinated and re-challenge group. Genes associated with Th2 pathway are shown in pink, genes associated with Th1 pathway are shown in green, and immune cells are highlighted with blue.

cytokines *Il4* and *Il13* in this group as measured by both nCounter technology and RT-qPCR (Supplementary Fig. S8). Although the correlation between the two measurements (RT-qPCR and nCounter) was moderate ($R^2 = 0.45$ for *Il4*, $R^2 = 0.19$ for *Il13*), both revealed the same trend early post infection (2 and 4 DPI) (Supplementary Fig. S8). Furthermore, the chemokine *Ccl22* was markedly increased (Fig. 7c). This chemokine is mainly expressed by macrophages and dendritic cells²⁶ and attracts Th2-polarized lymphocytes via their CCR4 receptor²⁷. Th1 pathway expression differed in kinetics between the vaccinated and the mock-vaccinated group, showing a faster recovery to baseline in the former group (Fig. 7b), which coincided with upregulation of several genes associated with Th1/Th17-response on 6 DPI and 8 (Fig. 7c). Similar to the first study, individually measured transcripts of *Ifng*, *Tnf*, *Il6* and *Il2* did not show clear differences between the vaccinated and the mock-vaccinated animals (Supplementary Fig. S9). The Th17 pathway was the least activated in the vaccinated group at 2 DPI, and overlapped with the mock-vaccinated group at later timepoints (Fig. 7b). In contrast, the Treg pathway score overlapped for the vaccinated and mock-vaccinated group early post infection (2 and 4 DPI), but showed a trend of faster recovery in the vaccinated group from 6 DPI onwards (Fig. 7b). Transcripts associated with the Th17 and the Treg pathways were heterogeneously represented, with some genes upregulated and some downregulated in the vaccinated group (Fig. 7c).

Next to the Th pathway-associated genes, a significant upregulation of a cluster of genes associated with immune cells was also observed in the vaccinated group, most prominently on 4 and 6 DPI (Fig. 7c). Of note, this coincided with the increased perivascular cuffing observed in this group (Fig. 6d). Transcripts associated with T-cells and cytotoxic cells were enriched mainly at 6 and 8 DPI, which correlated with the faster activation of the Th1 and the Treg pathways in vaccinated animals (Fig. 7b). Transcripts associated with neutrophils and macrophages were less abundant in the vaccinated group at 4 and 6 DPI, respectively. Given the pronounced cellular infiltration of the lungs of the hamsters in the vaccinated group at these time points, this finding most likely reflects changing ratios between cell populations, rather than decreased abundance of macrophages and neutrophils in absolute numbers.

Discussion

Vaccine Associated Enhanced Disease (VAED) is a well-described phenomenon in the context of formalin-inactivated whole virus vaccines against human respiratory syncytial virus (HRSV) and measles virus (MeV) used in the 1960s^{7,28}. However, a unified definition of this phenomenon remains challenging. In 2021, a case definition of the term "Vaccine Associated Enhanced Disease" was proposed by a group of experts within the Brighton Collaboration, summoned by the Coalition for Epidemic Preparedness Innovations (CEPI) in the context of developing safe vaccines for SARS-CoV-2 and other emerging pathogens¹. According to the definitions from this working group, a probable case of VAED in a previously seronegative vaccinated individual is characterized by the following criteria: (1) Laboratory confirmed infection with the pathogen targeted by the vaccine; AND (2) Clinical findings of disease involving one or more organ systems (a

case of VAED (vaccine-associated enhanced respiratory disease) if the lung is the primarily affected organ); AND (3) Severe disease as evaluated by a clinical severity index/score (systemic in VAED or specific to the lungs in VAED); AND (4) Increased frequency of severe outcomes (including severe disease, hospitalization and mortality) when compared to a mock-vaccinated population (control group or background rates); AND (5) Evidence of immunopathology in target organs involved by histopathology, when available, including among others: present or elevated tissue eosinophils in tissue and elevated pro-inflammatory Th2 cytokines in tissue (*Il4*, *Il5*, *Il10*, *Il13*) AND the absence of identified alternative etiology²⁹).

Early in the COVID-19 pandemic, it was disputed whether Syrian hamsters were a suitable model for studying VAED in the context of candidate SARS-CoV-2 vaccines. These doubts were based on previous results obtained while studying SARS-CoV infection in hamsters^{13,30}. Recently, a study in golden Syrian hamsters vaccinated with formalin-inactivated whole SARS-CoV-2-based vaccine preparation showed no evidence of enhanced pathology in vaccinated hamsters at 4 DPI²⁰. In that study, an unadjuvanted vaccine preparation was used, and neutralizing antibodies were measurable prior to challenge. In contrast, another study in golden Syrian hamsters designed to promote the occurrence of VAED by using a non-stabilized SARS-CoV-2 spike protein adjuvanted with aluminum hydroxide as a vaccine, did report VAED associated with up-regulation of Th2 cytokine genes (*Il4*, *Il5* and *Il13*), inadequate levels of neutralizing antibodies and presence of non-neutralizing antibodies²³. The results of this study are in line with the definition for VAED cited above, and with our own findings in the two hamster studies reported here. We consistently observed aggravated lung pathology post challenge, associated with increased perivascular infiltration of mononuclear cells and granulocytes, and the upregulation of Th2 cytokines (*Il4* and *Il13*) in lung tissue of vaccinated hamster when compared to naïve hamsters. We did not detect an increased severity or frequency of clinical outcomes. However, to our knowledge, clinical aggravation has never been reported in vaccinated as compared to mock-vaccinated animals in SARS-CoV-2 models.

In both studies, body weight loss in the mock-vaccinated hamsters was overall similar, with maximum weight loss during the period used for statistical analysis averaging 14.9% in the model development study and 15.9% in the kinetics study. However, the body weight loss in the 1x vaccinated group of the kinetics study was less pronounced than in the 1x high dose group of the model development study, (maximum weight loss average 5.8% vs. 12.0%) and body weight recovery started a day earlier—at 4 DPI instead of 5 DPI. This discrepancy could be due to various factors, including between-study variations, sample size, and potentially the sex of the animals. It has been demonstrated that body weight loss differs between male and female hamsters post SARS-CoV-2 challenge infection³¹. In our model development, both sexes were used, while in the kinetics study only females were included. This choice was made to reduce animal-to-animal variability, as the group size for each necropsy time point was small. For future experiments using this model as a control for VAED, it is essential to match the sex of the animals with those used in the candidate vaccine groups, and

ensure group sizes are sufficiently large to account for variability in the readout parameters.

In our first study, animals were sacrificed at 5 or 13 DPI. At 5 DPI, the vaccinated hamsters exhibited a transient increase in the severity of pathological lesions, compared with the mock-vaccinated hamsters. By 13 DPI, no clear histological differences were observed between the groups, although the vaccinated hamsters showed a slight trend toward higher histological scores. However, the limited number of animals per time point and the inclusion of only two necropsy time points made it challenging to fully elucidate the kinetics of the observed processes. Therefore, in the second study, the development of lung pathology was followed over time. It became evident that rather than the overall severity of histological lung lesions, the types of lesions and the kinetics of pathological changes distinguished the vaccinated from the mock-vaccinated hamsters. The pathological lesions associated with FIWV vaccination had accelerated kinetics, manifesting with faster exacerbation, followed also by faster recovery as compared with the mock-vaccinated group. An important exception to the overall trend of faster recovery in the vaccinated animals were the perivascular infiltrates, which remained most pronounced in these animals up to 6 DPI, and gene expression profiles showing enrichment of immune cell-associated transcripts up to 8 DPI. The perivascular infiltrates consisted of mononuclear cell and several granulocyte cell types (eosinophilic, heterophilic or neutrophilic). Eosinophils are known to play an important role in the vaccine-associated immunopathology of the lung. However, in hamsters, it is particularly challenging to distinguish eosinophils from other types of granulocytes. The predominant type of granulocyte in blood of hamsters are neutrophilic granulocytes³², which are also known as pseudo-eosinophils or heterophils, because their granules stain with eosin³³. True eosinophils compose only a small percentage of the blood cell fraction and differentiation from neutrophils based on their morphology is unreliable³⁴. Additional staining methods have been suggested to discriminate eosinophils from neutrophils/heterophils^{23,35}. However, we were unable to establish a satisfactory method for eosinophil-specific differentiation. Furthermore, dense inflammatory infiltrates in both naïve and vaccinated hamsters further complicated the differentiation between eosinophils and neutrophils. Therefore, we did not discriminate between the different types of granulocytes in the histology analysis. Overall, we observed more pronounced infiltrates in the perivascular space with an increase in eosinophilic and heterophilic/neutrophilic cell populations in the vaccinated hamsters as compared with the mock-vaccinated hamsters.

Concurrent with the accelerated lung histopathology, gene expression profiles revealed more prominent Th2 skewing of the immune response in the vaccinated compared with mock-vaccinated hamsters early after infection (2 and 4 DPI). This activation was associated with increased production of the Th2 cytokines *Il4* and *Il13*, and the chemokine *Ccl22*. Despite this early and stronger skewing of the immune response towards a Th2 phenotype, the vaccinated hamsters recovered faster in terms of Th1 and Treg regulation, and histological lesions observed in the lung. By 10 DPI, histological changes were largely resolved and expression of the genes associated with Th-pathways and immune cells were comparable in re-challenged, mock-vaccinated and vaccinated animals. This observation contrasts with results obtained in mice after challenge with either SARS-CoV or SARS-CoV-2, where enhanced lung histology accompanied by pronounced eosinophilic infiltration was observed at 10 DPI in association with vaccination^{22,36,37}, underscoring species-specific differences in the animal models used for preclinical studies. Intriguingly, in a recent work in ACE2-humanized mice, local and systemic upregulation of Th17 was reported at 7 DPI in animals vaccinated with the S1 and S2 extracellular domains of the SARS-CoV-2 Spike protein, adjuvanted with alum²⁴. This finding contrasts our results in hamsters. From all genes associated with differential T-cell regulation, the selected genes associated with the Th17 pathway were the most abundant (Supplementary table S5), yet the only difference between vaccinated and mock-vaccinated animals was observed very early post infection (at 2 DPI), when the Th17 pathway was the least activated in the vaccinated group. The observed difference could be a result

of species differences, dissimilar vaccines used, and the distinct challenge used in the mouse study, namely first a low dose, followed 3 days later by a high dose of the same challenge virus.

In our studies, we established the presence of binding, but the absence of neutralizing antibodies in the vaccinated hamsters. Antibody disease enhancement (ADE) mediated by vaccine-induced non-protective antibodies is well-studied for HRSV, measles and DENV (summarized by ref. 1). For SARS-CoV-2, in vitro evidence for antibody-mediated enhanced cell entry has been found in experiments with human lymphoid cell lines and in other cell lines expressing Fcγ receptor or hACE2 receptor (reviewed by ref. 38). In human macrophages however, despite Fcγ-mediated internalization of SARS-CoV-2, the virus is incapable of productive replication in those cells³⁸, arguing against the possibility of a direct macrophage-driven ADE. Furthermore, when antibodies found to be enhancing in vitro were administered to mice and NHP, no disease or pathology enhancement in vivo was observed³⁹. These results in preclinical models, together with studies proposing that antibody effector functions other than neutralization play a role in preventing ADE manifestation^{38,40–42}, suggest that the accelerated pathology observed in our study is not a sole result of the presence of non-protective antibodies. Rather, a combination of lack of neutralizing antibodies, a Th2-skewed immune response, and the presence of non-protective antibodies facilitating possible immune complexes formation seem to be a plausible explanation for the lung pathology in vaccinated hamsters. With respect to the nucleoprotein (N) and anti-N antibodies, it has been shown that the N protein has the ability of inducing macrophages to produce high levels of IL-6, one of the cytokines associated with severe disease in COVID-19 patients⁴³. Moreover, the N protein aggravates lung injury and promotes IL-1β and IL-6 secretion in mouse models⁴⁴. Anti-N antibodies enhanced the effect of N on IL-6 production by macrophages⁴⁵ and sera from patients with severe COVID-19 had high concentration of anti-N IgG⁴⁶. However, in our hamster model, only 3 vaccinated animals had detectable levels of anti-N binding antibodies prior to challenge. Although anti-N antibodies increased earlier in vaccinated hamsters, the overall kinetics followed the same slope as in mock-vaccinated hamsters. Moreover, we did not observe increased production of IL-6 on the transcriptional level in vaccinated as compared with mock-vaccinated animals. Collectively, these findings suggest that anti-N antibodies did not play a pivotal role in the accelerated lung pathology in our hamster model.

One point of attention indicated by Munoz et al. is the importance of methodically clearing challenge materials and vaccines from cellular debris, which may otherwise enhance reactogenicity in animal models and bias observations¹. In our study, significant effort was devoted to purifying the vaccine preparation from culture contaminants to avoid sensitization of vaccinated animals towards those contaminants, but the inoculum itself was administered unpurified. In that context, it cannot be ruled out entirely that the accelerated Th2-enhanced response is (partially) associated with sensitization towards inoculum contaminants. However, if that would be the case, a double vaccination regimen would be expected to manifest as stronger pathological response towards challenge infection, but we did not observe such a trend in our first study. Therefore, it is unlikely that sensitization towards inoculum contaminants can explain the Th2 polarization and the accelerated lung pathology in vaccinated hamsters. To avoid concerns about challenge inoculum purification, a standardized transmission model can be considered for future studies exploring VAED.

There are several limitations to this study. We chose to perform a gene expression survey with pre-selected genes, instead of complete unbiased transcriptomics analysis. The power of such a targeted survey is the focused inquiry of only a relevant group of genes of interest. At the time of selecting target genes for our study, Syrian hamster-specific gene annotations for either genome-wide or immunologically-focused transcriptional analysis were still largely unavailable. Therefore, some of the genes identified by Ebenig et al.²³ as potentially additional important players behind the VAED mechanism (i.e. *Il19* and *Ccl11*) or by Nouallies et al.⁴⁷ as genetic markers for immune cells were not included in our custom multiplexed hybridization panel. However, it is important to note that the key genes associated with Th

regulation are represented in our custom nCounter panel, including *Il4*, *Il5* and *Il13*, which are considered as the pivotal cytokines indicative of Th-2 skewing of the immune response⁴⁸. Therefore, we were able to gain insights into the Th-skewing of the treatment groups in the kinetics study. Another limitation of our study is the translatability of the obtained data in hamsters to the human situation. To this date, there is no evidence of vaccine-associated disease enhancement in humans following natural infection with SARS-CoV-2. Furthermore, a recent study⁴⁹ examined the risk of ICU admission and severe illness in hospitalized COVID-19 patients. Their findings revealed that vaccinated individuals experienced significantly lower disease severity, providing strong evidence against the occurrence of vaccine-associated enhanced disease (VAED). Given that COVID-19 vaccines have been administered on an unprecedented global scale, a significant occurrence of VAED would likely have been detected by now. The lack of such evidence strongly suggests that VAED is not a relevant risk in the context of COVID-19 vaccination. It is however important to have readily available models in which safety of new vaccines for SARS-CoV-2 or other pathogens can be tested¹.

In conclusion, our data support the hypothesis that Syrian hamsters are a suitable model for inducing VAED with FIWV adjuvanted with alum. The vaccination elicited spike-binding antibodies and virtually no neutralizing antibodies prior to challenge. Post challenge, animals did not display aggravation of clinical disease as compared with mock-vaccinated animals. VAED manifested with early upregulation of Th2 cytokines (*Il4* and *Il13*) and chemokines (*Ccl22*) and faster progression of immunopathology, characterized by more pronounced and prolonged perivascular infiltrates, and dominated by eosinophilic and heterophilic/neutrophilic cell species.

Materials and methods

Ethical statement

Wageningen Bioveterinary Research is authorized to perform animal experiments according to the Dutch Law on Animal Experiments (WoD) and in accordance with European legislations and guidelines. The current study was performed under project license no. AVD4010020209446 of the Dutch Central Authority for Scientific procedures on Animals (CCD). The experimental plan was approved by the Animal Welfare Body of Wageningen University and Research prior to the start of the in-life phase. Protocols were prepared in compliance with 3 R policies, and the study reports are presented in compliance with the ARRIVE guidelines⁵⁰.

Vaccine preparation

For production of the virus stock, Vero/hSLAM cells (Sigma-Aldrich, Merck, Darmstadt, Germany, Cat# 04091501-1VL) were used, cultured in minimum essential medium (Life Technologies, Carlsbad, CA, USA) supplemented with 4% heat-inactivated FBS (Sigma-Aldrich), 25 mM Hepes (Life Technologies) and geneticin (0.4 µg/ml) (Gibco, Thermo Fischer Scientific; Waltham, MA, USA). Production of the stock, preparation of the formalin-inactivated whole virus (FIWV) SARS-CoV-2 vaccine, and the subsequent purification and characterization of the FIWV have been described previously¹⁹. Prior to administration, frozen formalin-inactivated whole virus was thawed, diluted with phosphate buffered saline (PBS), and mixed 1:1 with 2% Alhydrogel (InvivoGen, Toulouse, France) to a final concentration of 0.5 µg vaccine antigen per dose (low dose) or 5 µg vaccine antigen per dose (high dose) for the first study, or to 5 µg vaccine antigen per dose for the second study. The same vaccine preparation was used for both studies described in this manuscript.

Viruses and cells

The virus used for inoculation in both studies was SARS-CoV-2 D614G, strain SARS-CoV-2/human/NL/Lelystad/2020⁵¹. In the first study, an undiluted virus stock prepared as previously described⁵¹ was used at a dose 10^{4.22} TCID₅₀ per hamster. For the second study, the virus stock was obtained following a second passage of the original isolate on Vero/hSLAM cells at MOI 0.0001. The culture medium consisted of MEM (Gibco, Thermo Fischer Scientific; Waltham, MA, USA, Cat# 21090),

supplemented with 2% FCS, 1% antibiotic/antimycotic, 1% L-glutamine, 1% Minimal Essential Medium Non-Essential Amino Acids (MEM-NEAA) (all from Gibco). Inoculations of hamsters were performed with undiluted virus stock at a dose of 10^{4.13} TCID₅₀ per hamster. Sequences of both virus stocks were determined by next generation sequencing and were identical to the original isolate, with no deletions or mutations in the furin cleavage site. For virus neutralization test, VERO-E6 cells (ATCC® CRL-1586™; Manassas, VA, USA) were used, cultured in MEM (Gibco, Cat# 21090), supplemented with 5% FCS, 1% antibiotic/antimycotic, 1% L-glutamine, 1% Minimal Essential Medium Non-Essential Amino Acids (MEM-NEAA) (all from Gibco).

Experimental design

For both studies, Syrian hamsters (*Mesocricetus auratus*), strain RjHan:AURA were obtained from Janvier, France. All hamsters were housed solitary in cages with open grids in one animal room under human BSL3 containment level. Water and food were provided ad libitum. Hamsters were monitored daily for their general health from the day of arrival until the end of the study and were allowed to acclimatize for at least 7 days before subjected to any study-related handlings. Vaccines and mock-treatment (phosphate buffered saline (PBS)) were administered intramuscularly (IM) by injection of 100 µL in the left hind leg. Where relevant, booster vaccination was administered IM in the right hind leg. Body weights of all hamsters were measured approximately twice per week during the acclimatization and vaccination period. Blood drawn from the retroorbital sinus and challenge infection with SARS-CoV-2 via the intranasal (IN) route were performed under general anesthesia with 0.15 mg/kg medetomidine (Sedastart, ASTfarma; Oudewater, The Netherlands) and 100 mg/kg ketamine (Narketan, Vetoquinol; Breda, The Netherlands). The anesthesia was antagonized with atipamezole (Sedastop, ASTfarma; Oudewater, The Netherlands). Animals were euthanized by anesthesia with 0.25 mg/kg medetomidine and 200 mg/kg ketamine, followed by exsanguination. Definition of humane endpoints (HEPs) were described previously⁵¹.

VAED model development: establishing vaccination conditions that result in VAED (Fig. 1, upper panel).

A total of 60 golden Syrian hamsters, (30 male and 30 female), 6–8 weeks of age at arrival, were used for the study. Hamsters from the same sex were assigned to one of 5 treatment groups ($n = 6$ males and $n = 6$ females per group) based on equal distribution of body weights across groups and subgroups (per day of euthanasia). One group of hamsters was immunized with a low (0.5 µg) dose, and one with a high (5 µg) dose of FIWV vaccine 33 days prior to challenge (−33 DPI) and then at −14 DPI (2x low dose and 2x high dose groups, respectively). Two other groups received either a single low or high dose of the same vaccine at −14 DPI only (1x low dose and 1x high dose, respectively). The fifth group received a vaccination with PBS at −14 DPI and served as mock-vaccinated control. All vaccinations were applied in a volume of 100 µl via the intramuscular (IM) route. Thirteen days post last vaccination (−1 DPI), $n = 4$ hamsters of each group were sacrificed for necropsy and served as unchallenged controls. The rest of the hamsters ($n = 8$ hamsters per group) were inoculated with SARS-CoV-2 at 0 DPI. From the inoculated hamsters, $n = 4$ per group were euthanized at 5 days post inoculation (5 DPI) and the other $n = 4$ animals per group were sacrificed at 13 DPI. During the challenge phase, body weights were measured daily. In addition, activity of the hamsters to be sacrificed on 13 DPI ($n = 4$ per group) was monitored daily by means of individual activity tracking wheels (Tecnilab BMI, Someren, The Netherlands)⁵¹. The running wheels were connected to an automatic rotation counter. Counts were recorded once per 24 h at approximately the same time of day and the counters were reset to 0. One complete wheel rotation corresponded to 4 counts. Serum samples were collected on the day prior to each vaccination (−34 and −15 DPI), two days prior to challenge (−2 DPI) and on both necropsy days (5 and 13 DPI) by retro-orbital puncture under general anesthesia. From the hamsters that were euthanized at -1 DPI, serum samples were taken during necropsy. At

necropsy, the left lung lobe was weighed and collected for pathological investigation, while cranial, medial and caudal right lung lobes were collected for viral load. The cardiac lung lobe was collected for cytokine measurements.

One hamster of the 1x high dose vaccine group reached a HEP on 7 DPI, showing depression, abdominal breathing and 19% body weight loss, and it was euthanized. This same animal also exhibited nonspecific symptoms (ruffled fur, hunched posture, and reduced alertness) on the day of challenge infection, prior to administration of the anesthesia. Furthermore, it was also one of the smallest in the study and consistently had the lowest body weight from -5 DPI until reaching HEP at 7 DPI, except for two measurements (0 DPI and 3 DPI). We cannot rule out the possibility that an unknown underlying condition contributed to the deterioration of the this one hamster post-challenge. Therefore, data from this hamster was excluded from the study.

VAED kinetics: investigation of the kinetics of VAED during infection (Fig. 1, lower panel). A total of 45 female golden Syrian hamsters, 8 weeks of age at arrival, were assigned to one of 3 treatment groups ($n = 15$ animals per group in total) based on equal distribution of body weights across groups and subgroups (per day of euthanasia). One group of hamsters was inoculated IN with SARS-CoV-2 (re-challenge group) at -22 DPI. To confirm successful infection in this group, oropharyngeal swabs (MW100, Medical Wire, Corsham, UK) were collected every 2 to 3 days, starting 3 days prior to inoculation until 10 days post inoculation. Hamsters from the other two groups were injected IM at -14 DPI with either vaccine (5 μ g vaccine antigen) or with PBS (1x vaccinated and mock-vaccinated groups respectively), both in a volume of 100 μ l. Two weeks post vaccination (vaccinated and mock-vaccinated groups) and approximately 3 weeks post first challenge (re-challenge group), all hamsters were inoculated IN with SARS-CoV-2 (0 DPI). At 2, 4, 6, 8 and 10 DPI, $n = 3$ hamsters per group were euthanized to perform necropsies and to collect lung tissue. The left lung lobe was collected for pathological analysis and the right caudal and cardiac lobes for virological and mRNA expression analysis (Nanostring® nCounter technology, Seattle, WA, USA). During the challenge phase, body weights were measured once daily starting 5 days prior to challenge and ending on the day of necropsy. Serum samples were collected before vaccination, prior to challenge and during necropsy by retroorbital puncture under general anesthesia.

Pathological evaluation of lung tissue and immunohistochemistry

The left lung lobe was removed and weighed, and the weight was expressed as percentage of the body weight measured on the day of challenge (relative lung weight). Subsequently, the left lung lobe was gently inflated and immersed in 10% neutral buffered formalin, fixed for 14 days and embedded in paraffin, sectioned at 5 μ m and stained with hematoxylin and eosin (H&E) for histological examination. The percentage of the total extent of the left lung lobe that was microscopically affected by SARS-CoV-2-related lesions, was estimated in a blinded fashion by a board-certified veterinary pathologist. Three blinded estimates with different order of slides were performed and averaged for a final score. For the model development study, a section from the lung of each hamster from both 5 and 13 DPI was evaluated by a second, independent board-certified veterinary pathologist in a blinded fashion. Percentage of affected lung tissue was calculated using digital image analysis (Nikon NIS-Ar software, Tokyo, Japan). The agreement between the scores assigned by both pathologists was assessed by correlation analysis (GraphPad (San Diego, CA, USA) software Prism v. 9.4.0). The severity and characteristics of the (histo)pathological lesions were scored semi-quantitatively as described previously⁵¹ with slight modifications as shown in Table 1a. To account for the different scales of the 6 individual parameters that were scored, all scores were normalized by multiplying by a correction factor (4/highest score of each scale). Normalized scores were used to calculate cumulative (“sum”) scores for visual representation and for statistical analysis. The severity and characteristics of

the lung lesions were also analyzed by the second pathologist in a blinded fashion and in a descriptive way.

SARS-CoV antigen expression was evaluated with immunohistochemistry (IHC) on formalin-fixed and paraffin-embedded (FFPE) lung tissue sections. Heat-induced epitope retrieval (HIER) method was used to prepare slides for IHC stain as previously described⁵¹. Briefly, after routinely dewaxing and endogenous peroxidase quenching (methanol/0.3% H_2O_2), the sections were heated for 15 min at 100 °C (Pascal, Dako, Agilent, Santa Clara, CA, USA pressure cooker) in 10 mmol citrate buffer pH 6.0 (Dako, Cat# S1699). The slides were blocked with 10% goat serum (Dako) and stained with primary polyclonal rabbit anti-SARS-CoV NucleoProtein (Sino Biological, Beijing, China, Cat# 40163-T62) and secondary HRP-conjugated anti-rabbit reagent (Envision + Single Reagent, Dako, Cat# K4003). For visualization, the 3,3'-diaminobenzidine (DAB) (Dako, Cat# K3468) substrate was used. Slides were counterstained with haematoxylin. The semiquantitative scoring system for the level of SARS-CoV-2 virus antigen expression in the lungs is shown in Table 1b (Level of antigen expression).

Oropharyngeal swab sampling and analysis

Following sampling, the swabs were directly submerged in 2 ml of complete culture medium and kept on melting ice until transport to the lab and freezing at ≤ -70 °C. Upon thawing, swab samples were vortexed, and 200 μ l of the sample was mixed with 211 μ l lysis master mix, consisting of 200 μ l lysis buffer supplemented with 1 μ l Poly-A RNA and 10 μ l Proteinase K solution (Molgen Pureprep Pathogens Kit, Utrecht, The Netherlands). Lysis buffer-inactivated samples were stored at ≤ -15 °C until RNA isolation and PCR analysis. RNA from oropharyngeal swabs was isolated by an automated robot system (PurePrep 96, Molgen), using the Pureprep Pathogens RNA isolation kit (Molgen) according to manufacturer instructions.

Assessment of viral genome loads

In the VAED model development study, the collected cranial, medial and caudal right lung lobes were kept on melting ice until initial storage at ≤ -70 °C. Upon further processing, tissue samples were weighed, thawed and homogenized in 6 mL Earl's MEM (Gibco), supplemented with 1% antibiotic/antimycotic (Gibco), using DT-20 Tubes with Rotor Stator Element (Thermo Fisher Scientific) and an Ultra-Turrax® homogenizer (IKA; Staufen, Germany). The tissue homogenates were centrifuged for 15 min at $3400 \times g$ at 4 °C and 85 μ l of the supernatant was mixed with 255 μ l Trizol LS and stored at ≤ -15 °C. In the VAED kinetics study, the right cranial and middle lung lobes were directly snap-frozen in liquid nitrogen and kept on dry ice until initial storage at ≤ -70 °C. Upon further processing, snap-frozen lung tissue samples were weighed and homogenized in 5 mL Trizol by an Ultra-Turrax® homogenizer. The tissue homogenate was centrifuged for 15 min at $3400 \times g$ at 4 °C and supernatants were aliquoted and stored at ≤ -15 °C. RNA extraction from the lung suspensions in Trizol was performed manually with individual columns of the Direct-zol Miniprep Kit (Zymogen, Irvine, CA, USA), following manufacturer instructions. The isolated RNA samples were stored at ≤ -70 °C until further use for analysis by SARS-CoV-2 qPCR to assess total viral RNA levels and subgenomic RNA levels. Viral RNA loads were measured by qPCR essentially as previously described⁵¹, using primer/probe sets for both total viral E-gene PCR⁵² and subgenomic PCR (sgPCR)²⁵. The former PCR detects all positive RNA species (genomic and subgenomic) containing the E-gene sequence, while the latter detects only the subgenomic species generated during active virus replication.

Cytokine PCR

Lung tissue samples were used for analyses with RT-qPCR to assess mRNA expression levels of Th1 (*Ifng*, *Tnfr*, *Il2*, *Il6*) and Th2 (*Il4*, *Il13*) cytokines. To that end, in the model development study the accessory lung lobe was submerged in 1 mL Trizol in a vial pre-filled with lysing beads (matrix D, MP Biomedicals, Irvine, CA, USA). Subsequently the lobe was grinded using a Fastprep-24 instrument (MP Biomedicals) and then stored at ≤ -70 °C until

Table 1 | Scoring system for the severity and characteristics of (a) lung gross pathology and histopathology (H&E staining) and (b) for level of SARS-CoV-2 antigen expression in the lungs (modifications in comparison with the previously described system⁵¹ are indicated with cursive)

(a) Parameter	Score	Extent of lesions
General scores		
Gross pathology	0	No macroscopical changes
	1	Focal discoloration of the lung in <15% of lung surface
	2	Multifocal discoloration of approximately 15–40% of lung surface
	3	Multifocal discoloration affecting approximately 40–70% of lung surface
	4	Whole lung affected in >70% of lung surface
Extent lung histopathology (general score, percentage) (H&E)	0	No changes
	1	Focal to multifocal (<15% of tissue)
	2	Multifocal (15–40% of tissue)
	3	Multifocal to coalescing discoloration (40–70% of tissue)
	4	Diffuse (>70% of tissue)
Individual histological parameters (severity)		
Alveoli - (thickening alveolar wall, type II pneumocyte proliferation, inflammatory cells alveoli)/ interstitial pneumonia	0	No changes
	1	Focal to multifocal (<20% of tissue)
	2	Multifocal (20–50% of tissue)
	3	Multifocal to coalescing (>50% of tissue)
Bronchi and bronchiole	0	No changes
	1	<i>Peribronchiolar infiltrate or in lumina with no or mild epithelial degeneration < 20% of bronchi/bronchioles</i>
	2	<i>Peribronchiolar infiltrate or in lumina with mild to moderate epithelial degeneration > 20–50% of bronchi/bronchioles</i>
	3	<i>Peribronchiolar infiltrate or in lumina with severe epithelial degeneration and necrosis > 50% of bronchi/bronchioles</i>
Blood vessels	0	No changes
	1	<i>Perivascular clear spaces (edema) with only mild infiltrates of inflammatory cells > 15% of large blood vessels</i>
	2	<i>Clear perivascular cuffing in > 15–30% of blood vessels, with occasionally presence of inflammatory cell in blood vessel wall without clear degeneration</i>
	3	<i>Extensive perivascular cuffing often of more than 5 cell layers, also in large arteries with clear infiltrates of inflammatory cells in blood vessel walls</i>
Hemorrhage/hemosiderophages (macrophages with hemosiderin)	0	No hemorrhage/hemosiderophages
	1	Mild focal to multifocal hemorrhage/hemosiderophages
	2	Moderate to severe multifocal hemorrhage/hemosiderophages
(b) Parameter	Score	Extent of lesions
Level of antigen expression (IHC)	0	No staining
	1	<i>Focal or multifocal staining (<5 foci) en < 15% of tissue</i>
	2	<i>Multifocal staining in 15–40% of the tissue</i>
	3	<i>Multifocal to coalescing staining in > 40–70% of the tissue</i>
	4	<i>Diffuse staining in > 70% of the tissue</i>

further processing. In kinetics study, the right cranial and middle lung lobes were used and were processed as described above (“Assessment of viral genome loads”). RNA extraction in both studies was performed as described above, using individual columns of the Direct-zol Miniprep Kit (Zymogen), according to manufacturer instruction, including a DNase step performed on the columns to degrade host DNA. To prepare cDNA, 200 ng RNA per sample (model development study) or 100 ng RNA (kinetics study) was used as an input for a reverse transcription reaction, using the Superscript IV First-strand synthesis system Thermo Fisher Scientific, Waltham, MA, USA), following the manufacturer’s instructions. The cDNA reaction was performed on an Applied Biosystems 7500 Instrument with the following temperature conditions: 10 min at 23 °C (annealing step); 10 min at 50 °C (reverse transcription step); 10 min at 80 °C (denaturation); 4 °C (termination). For normalization, the reference genes *RPL18* and *Ywhaz* were

selected, following an initial screening of 6 reference genes (*Rpl18*, *Rpl13*, *Pp1a*, *Ywhaz*, *B-actin*, *B2m*) and determining the two most stable ones with the GeNex Software v.7 (MultiD Analyses AB, Göteborg, Sweden). For the screening, half of the samples were used in the first study and selection was confirmed on one third of the samples in the second study. Primer sequences and cycling conditions are provided in Tables 2 and 3. Primers were ordered at Biogio (Nijmegen, The Netherlands). All PCRs were performed using Power SYBR Green PCR Master mix (Thermo Fisher Scientific) according to manufacturer’s instructions with 1:10 diluted sample cDNA and primer concentrations as indicated in Table 2 in a total reaction volume of 20 µl or 50 µl in the first or second study, respectively. All PCRs were performed on an Applied Biosystems 7500 Instrument.

Relative expression of the genes of interest (GOI) was determined with the $\Delta\Delta CT$ method⁵³, using *Rpl18* and *Ywhaz* as reference genes for

Table 2 | List of primer sequences, final primer concentrations and temperature conditions of the qPCRs

Gene	Primer concentration (µM)	Amplification temperature (°C)	Forward sequence	Reverse sequence	Sequence source	NCBI reference number of the transcript
<i>Rpl18</i>	0.25	58	GTTTATGAGTCGCCTAAACCG	TGTTCTCTCGGCCAGGAA	Zivcec et al. Journal of Immunological methods (2011)	XM_005084699.3
<i>Ywhaz</i>	0.125	60	GAAGCGGAAGCAGGAGAAG	TATTTGTGGACAGCAATGGA	Self-developed, using Primer 3 software (on-line)	AY569127.1
<i>Il6</i>	0.5	62	CCTGAAAGCACTTGAAGAATTC	GGTATGCTAAGGCACAGCACACT	Self-developed, using Primer 3 software (on-line)	XM_005087110.2
<i>Il13</i>	0.075	60	GCACCTCTGGGTGACCGTAGT	GCCCTCTGGTCTTGTGTGAT	Self-developed, using Primer 3 software (on-line)	XM_005067910.3
<i>Tnf</i>	0.25	60	TGAGCCATCGTGCCAAATG	AGCCCGTCTGCTGGTATCAC	Espitia et al. BMC Immunology 2010	XM_005086799.3
<i>Irfng</i>	0.125	63	TGTTGCTCTGCCCTCACTCAGG	AAGACGAGTCCCTCCCATTC	Espitia et al. BMC Immunology 2010	NM_001281631
<i>Il4</i>	0.075	60	ACCGAGATGGTGTGTACCAGA	CACAGGGTCACCTCATGTTG	Self-developed, using Primer 3 software (on-line)	XM_005067769.2
<i>Il2</i>	0.125	60	AGTGCACCCACFTCAAGCTC	GCCFTTGGGCATGTAAAA	Self-developed, using Primer 3 software	NM_001281629.1

Table 3 | Cycling conditions for the qPCRs

Stage	Repetitions	Temperature	Time
1	1	95.0 °C	10:00
2	40	95.0 °C	0:15
		XX.0 °C ^a	1:00
3 ^b (Dissociation)	1	95.0 °C	0:15
		60.0 °C	1:00
		95.0 °C	0:15
		60.0 °C	0:15

^aThis temperature is primer-specific and was optimized for each primer set. The relevant temperatures are listed in Table 2 (Amplification temperature).

^bStep 3 was used to generate dissociation curves. Quality of the PCRs and the generated fragments were evaluated per PCR run based on the melting curves. Samples that had PCR products with melting temperatures different than the expected PCR product were excluded from the analysis.

normalization. This method generates a unit-free number indicating expression of the GOI relative to a reference gene, taking variations among PCR plates into consideration. Before normalizing the GOI, the ΔCt values obtained for the two reference genes were averaged. Standard curves for each gene were prepared by 5-fold serial dilutions of a sample pool, including pre-selected samples mixed in equal amounts (*Rpl18*, *Ywhaz* and *Tnf*) or the sample pool was spiked with 5-fold serial dilutions of a synthetic DNA fragment (synthesized by GenScript Biotech, Piscataway, NJ, USA), encompassing the generated by PCR amplicon (*Il2*, *Il4*, *Il6*, *Il13* and *Irfng*). A standard curve was included on each PCR test plate.

Virus neutralization test

Serial 3-fold dilutions of sera were prepared in duplicates, starting at 1:10 initial dilution. A standard dose of ~100 TCID₅₀ of SARS-CoV-2/human/NL/Lelystad/2020 was mixed with the serum dilutions and incubated for 1 h. Subsequently, VERO-E6 cells were added to the mixture, at a density of 2 × 10⁴ cells/well. The plates were incubated for 4 days at 37 °C and 5% CO₂, after which cell monolayers were fixed with 4% formaldehyde, followed by fixation with pure methanol (kept at -20 °C) for cell permeabilization. Cell monolayers were then washed 3 times with PBS and stored at 4 °C until staining with an immunoperoxidase monolayer assay to visualize viral antigen, as described previously⁵¹. Briefly, cell monolayers were stained using primary anti-SARS-CoV-2 S1 (Wuhan strain) polyclonal antibody (custom-made by Davids Biotechnologie GmbH and obtained by immunization of rabbits with S1 protein; kindly provided by Dr. Berend Jan Bosch and Dr. Wentao Li, University of Utrecht, The Netherlands) and secondary HRP-conjugated anti-rabbit antibody (DAKO Cat# P0448). Both antibodies were diluted in PBS supplemented with 5% horse serum and incubated with the cell monolayer for 1 h at RT. Between the incubation steps, cell monolayers were washed 3 times with PBS, supplemented with 0.5% Tween-80. Staining was visualized following 30–40 min incubation with AEC substrate (4 mg/ml AEC in DMSO), freshly dissolved in substrate buffer (0.05 M NaAc buffer, pH adjusted to 5.0 using 0.05 M HAC) in the following manner: 19 mL substrate buffer + 1 mL 4 mg/mL AEC + 50 µL 3% H₂O₂. Evaluation of staining was performed using a standard light microscope.

The titer of each duplicate was determined as the average of the reciprocal value of the last dilution that showed ≥50% neutralization (lack of staining) in the well, evaluated by eye. The detection limit of the assay in this experimental setting was a titer of 5.7. All samples with undetectable titer were attributed a titer of 3.3.

Enzyme-linked immunosorbent assay (ELISA)

Anti-N and anti-S total IgG titers were determined by end-point dilutions of serum samples using a custom ELISA test. ELISA plates (medium bind, Greiner Bio-One, Krensmünster, Austria) were coated with 50 ng/well of either N or S protein (40588-V08B and 40589-V08B1 respectively, both purchased from Sino Biological, Beijing, China), dissolved in coating buffer (0.05 M Na₂CO₃ and 0.05 M NaHCO₃, pH 9.6) overnight at 4 °C. Blocking

was performed with StabilBlock (Surmodics, Eden Prairie, MN, USA) blocking buffer for 1 h at 37 °C. Test sera and the secondary antibody were diluted in dilution buffer (PBS, supplemented with 0.05% Tween 20 and 5% bovine serum albumin, sterile filtered with 0.45 µm filter) and incubated on the plates for 1 h at 37 °C with gentle agitation. Serum samples were serially diluted (2-fold dilution step), starting at dilution 1:50 (low positive sera), 1:200 (mid positive sera) or 1:1600 (high positive sera), based on a pilot test. As secondary antibody, anti-hamster IgG (Thermo Fischer Scientific Cat# HA6007) was used. For color development, TMB substrate (ImmunoChemistry Technologies, Davis, CA, USA) was added to the plates and incubated for 15 min at room temperature. Reaction was stopped with 0.5 M sulfuric acid and OD values were measured at 450 nm on a SpectraMax ABS Plus spectrophotometer (VWR; Radnor, PA, USA). All reagents were added to the ELISA plate wells in a volume of 100 µl (except the blocking solution, which was added in a volume of 300 µl). Between all incubation steps, the plates were washed 3 times with wash buffer (distilled water, supplemented with 0.05% Tween 20).

On each plate, the same negative and positive control were taken along in duplicates. These controls consisted of pooled sera obtained from previous experiments involving naive hamsters or hamsters recovered from SARS-CoV-2 infection, respectively. The negative control was diluted 1:50 and the positive control was diluted 1:250 (N-ELISA) or 1:500 (S-ELISA). The positive and negative controls were used to determine an S/P (sample/positive control) ratio for each sample according to the formula:

$$SP = (OD_SAMPLE - OD_NEG)/(OD_POS - OD_NEG)$$

For determination of the cut-off, nine pools were prepared from the serum samples obtained prior to vaccination of the hamsters from the respective experiment. These pools were diluted 1:50 and taken along on each plate. The cut-off of the ELISA was defined as the average S/P ratio of these pools plus 3x the standard deviation (SD). The ELISA titers of the tested sera were determined as the \log_2 value of the last serum dilution that showed an S/P ratio above the detection limit. Samples for which the starting dilution of 1:50 was negative were assigned the \log_2 value of one (theoretical reciprocal dilution step lower (1:25)).

Gene expression analysis in lung samples on the nCounter® platform

Digital nCounter® technology (NanoString Technologies) was used to assess mRNA expression levels of selected genes ($n = 128$) associated with Th1, Th2, Th17, and Treg pathways, and with genes associated with different immune cell types in hamster lungs. Custom nCounter panel selection was based on human and/or mouse genes from relevant pathway annotations in the human CAR-T (Chimeric antigen receptor T-cell) Characterization Panel (NanoString Technologies, Seattle, WA, USA), as well as on genes related to different immune cell types based on available literature for mice. In addition, $n = 3$ reference genes identified as stable/suitable based on previous qRT-PCR analyses were included for normalization purposes (*Rpl13*, *Rpl18*, and *Ywhaz*). Hamster-specific probes for transcripts homologous to the selected genes were designed and manufactured by NanoString Technologies, resulting in a custom hamster Code Set.

Total RNA was isolated from hamster lungs as described under “Assessment of viral genome loads”. RNA concentrations were quantified with a Qubit™ RNA HS Assay Kit on a Qubit® 2.0 Fluorometer (Invitrogen) and the percentage of RNA fragments >200 nucleotides (“DV200”) was determined with an RNA screen tape on an Agilent Technologies 220 TapeStation. Except for two samples from the mock-vaccinated group at 4 DPI (22.8% and 29.7%), the DV200 was >35% (range 35.1%–91.2%).

Multiplexed hybridization reactions were performed by Prof. Stephen Gordon and Dr. John A. Browne on an SFI-funded nCounter®MAX Analysis System (NanoString Technologies) at the UCD Veterinary Sciences Centre (Dublin, Ireland), according to manufacturer’s guidelines and as originally described by Geiss et al.⁵⁴. Hybridization reactions contained 300 ng of total RNA in a 5 µl volume (except for all DPI 2 samples and DPI 4 samples of the re-challenge group, which contained 100 ng), as well as

fluorescent barcode-labeled (reporter and capture) probes for endogenous and reference genes, six pairs of positive control probes, and eight pairs of negative control probes. Hybridized probes were loaded onto cartridges ($n = 12$ per run) and imaged on an nCounter® MAX instrument.

Analysis of raw RCC (Reporter Code Count) files was performed using nSolver Analysis Software (version 4.0) and nCounter Advanced Analysis Plugin (version 2.0.134). The analysis was run with standard settings, and included normalization, differential expression, and pathway scoring modules. Low count data were not excluded from the analysis. Automatic normalization of raw counts based on housekeeping (reference) gene abundance was performed by the software, leading to exclusion of *Rpl13* as normalization probe. A probe annotation file for pathway enrichment analysis was provided by NanoString Technologies and was based on the nCounter® CAR-T characterization and host response panels. During basic analysis, all samples passed standard QC requirements regarding imaging, binding density, and positive control linearity.

To analyze differential expression (DE), samples from all three treatment groups were analyzed separately per necropsy day ($n = 9$) with the same settings described above. Either mock-vaccinated or re-challenge groups were used as categorical reference (baseline) in the ‘fast/recommended’ DE analysis module which fits all genes with a negative binomial model and fold changes as well as univariate p values were calculated by the software.

Normalized count data and pathway scores were visualized with GraphPad Prism. The web app ClustVis (<https://biit.cs.ut.ee/clustvis/>)⁵⁵ was used to for Principal Component Analysis (PCA) and generation of heatmaps. For heatmaps, normalized expression counts were $\ln(x)$ -transformed, centered around the mean per gene, and unit variance scaling was applied to rows. Rows were clustered using Manhattan distance and average linkage.

Statistics

Analysis of the relative body weight losses for both studies was performed on the data between 5 DPI and 7 DPI for the hamsters present in the study up to 7 DPI (model development study: $n = 4$, subgroup sacrificed on 13 DPI; kinetic study: $n = 6$, subgroups sacrificed on 8 and 10 DPI). This time window was chosen because it encompasses the period with the largest body weight loss in the control mock-vaccinated group. Each hamster’s relative body weight was quantified by calculating the area under the curve (AUC). Between-group comparisons of the AUCs were made with one-way analysis of variance (ANOVA).

Activity wheel count analysis (first study) was performed on the data between 7 DPI and 10 DPI. This time window was chosen because it encompasses the period of activity recovery following the challenge-induced activity reduction. Data from 9 DPI was excluded from the analysis, because of an unexpected dip of activity in all groups, which was attributed to technical issue of unknown origin in the animal facility. Activity was analyzed by estimating the activity AUC and between groups comparisons were made by one-way ANOVA. The analysis was performed on log-transformed counts.

Group means of the VNT titers, lung pathology parameters (relative lung weights, extent of lung histopathology lesions, severity of histopathology lung lesions sum scores), viral loads (total E gene PCR) and cytokine data for the model development study were compared using two-way ANOVA, where DPI, group and interaction between DPI and group were assessed. Group means of the lung viral loads, as measured by sub-genomic RNA PCR at 5 DPI were compared with one-way ANOVA, since all values at 13 DPI were “0”. ELISA antibody titers for the kinetics study on 0 DPI of the vaccinated and the re-challenged group were compared with a (non-parametric) Mann-Whitney test.

In all cases where ANOVA was used, multiple comparisons were performed following a significant ANOVA test. ANOVA was applied with relaxed rule for data normality and variance equality. One-way ANOVA was followed by a Dunnett’s multiple comparison test between the control group (mock-vaccinated) and each of the treatment groups (first study) or between the vaccinated group and the two control groups (re-challenge and

Mock-vaccinated, second study). Two-way ANOVA was followed by a Dunnett's multiple comparison test (to determine differences between the control group (mock-vaccinated) and each of the treatment groups per necropsy day) or by Sidak's multiple comparison's test (to test for change over time within a group).

To compare changes in kinetics of serology titers, pathological parameters and Th-pathways over time among groups in the kinetics study, a multivariate linear regression model (interaction Group:time) was used. To account for non-linear changes in time, we introduced natural spline terms to the time variable. Pairwise comparisons between the groups were corrected using the Tukey method.

As a standard, an alpha of 0.05 and two-tailed tests were used. For all cases when multiple comparisons were made, the *p* value was corrected for multiple comparisons.

The ANOVA and the non-parametric tests were performed with GraphPad (San Diego, CA, USA) software Prism v. 9.4.0, and the multivariate linear regression modeling was performed with software R version 4.2.2 (Team R.C. R: A Language and Environment for Statistical Computing. Available online: <https://www.R-project.org/>).

Data availability

All data that were used to support the conclusions have been included in the manuscript and the "Supplementary Materials" file. nCounter raw data and normalized count tables as well as source data for Fig. 7c and Supplementary Fig. S7 are provided in the "Supplementary Data 1" file.

Received: 13 October 2024; Accepted: 12 May 2025;

Published online: 04 July 2025

References

- Munoz, F. M. et al. Vaccine-associated enhanced disease: case definition and guidelines for data collection, analysis, and presentation of immunization safety data. *Vaccine* **39**, 3053–3066 (2021).
- Kim, H. W. et al. Respiratory syncytial virus disease in infants despite prior administration of antigenic inactivated vaccine. *Am. J. Epidemiol.* **89**, 422–434 (1969).
- Delgado, M. F. & Polack, F. P. Involvement of antibody, complement and cellular immunity in the pathogenesis of enhanced respiratory syncytial virus disease. *Expert Rev. Vaccines* **3**, 693–700 (2004).
- Bigay, J., Le Grand, R., Martinon, F. & Maisonnasse, P. Vaccine-associated enhanced disease in humans and animal models: lessons and challenges for vaccine development. *Front. Microbiol.* **13**, 932408 (2022).
- Smatti, M. K., Al Thani, A. A. & Yassine, H. M. Viral-induced enhanced disease illness. *Front. Microbiol.* **9**, 2991 (2018).
- Gartlan, C. et al. Vaccine-associated enhanced disease and pathogenic human coronaviruses. *Front. Immunol.* **13**, 882972 (2022).
- Polack, F. P. Atypical measles and enhanced respiratory syncytial virus disease (ERD) made simple. *Pediatr. Res.* **62**, 111–115 (2007).
- Moghaddam, A. et al. A potential molecular mechanism for hypersensitivity caused by formalin-inactivated vaccines. *Nat. Med.* **12**, 905–907 (2006).
- Brewer, J. M. (How) do aluminium adjuvants work?. *Immunol. Lett.* **102**, 10–15 (2006).
- HogenEsch, H. Mechanisms of stimulation of the immune response by aluminum adjuvants. *Vaccine* **20**, S34–S39 (2002).
- Wang, Q. et al. Correction: Immunodominant SARS coronavirus epitopes in humans elicited both enhancing and neutralizing effects on infection in non-human primates. *ACS Infect. Dis.* **6**, 1284–1285 (2020).
- Bolles, M. et al. A double-inactivated severe acute respiratory syndrome coronavirus vaccine provides incomplete protection in mice and induces increased eosinophilic proinflammatory pulmonary response upon challenge. *J. Virol.* **85**, 12201–12215 (2011).
- Tseng, C. T. et al. Immunization with SARS coronavirus vaccines leads to pulmonary immunopathology on challenge with the SARS virus. *PLoS ONE* **7**, e35421 (2012).
- Deming, D. et al. Vaccine efficacy in senescent mice challenged with recombinant SARS-CoV bearing epidemic and zoonotic spike variants. *PLoS Med.* **3**, e525 (2006).
- Yasui, F. et al. Prior immunization with severe acute respiratory syndrome (SARS)-associated coronavirus (SARS-CoV) nucleocapsid protein causes severe pneumonia in mice infected with SARS-CoV. *J. Immunol.* **181**, 6337–6348 (2008).
- Liu, L. et al. Anti-spike IgG causes severe acute lung injury by skewing macrophage responses during acute SARS-CoV infection. *JCI Insight* **4** <https://doi.org/10.1172/jci.insight.123158> (2019).
- Agrawal, A. S. et al. Immunization with inactivated Middle East Respiratory Syndrome coronavirus vaccine leads to lung immunopathology on challenge with live virus. *Hum. Vaccin. Immunother.* **12**, 2351–2356 (2016).
- Li, K. et al. Single-dose, intranasal immunization with recombinant parainfluenza virus 5 expressing Middle East Respiratory Syndrome coronavirus (MERS-CoV) spike protein protects mice from fatal MERS-CoV infection. *mBio* **11**, <https://doi.org/10.1128/mBio.00554-20> (2020).
- Bewley, K. R. et al. Immunological and pathological outcomes of SARS-CoV-2 challenge following formalin-inactivated vaccine in ferrets and rhesus macaques. *Sci. Adv.* **7**, eabg7996 (2021).
- Li, C. et al. Absence of vaccine-enhanced disease with unexpected positive protection against severe acute respiratory syndrome coronavirus 2 (SARS-CoV-2) by inactivated vaccine given within 3 days of virus challenge in Syrian Hamster model. *Clin. Infect. Dis.* **73**, e719–e734 (2021).
- DiPiazza, A. T. et al. COVID-19 vaccine mRNA-1273 elicits a protective immune profile in mice that is not associated with vaccine-enhanced disease upon SARS-CoV-2 challenge. *Immunity* **54**, 1869–1882.e1866 (2021).
- Iwata-Yoshikawa, N. et al. A lethal mouse model for evaluating vaccine-associated enhanced respiratory disease during SARS-CoV-2 infection. *Sci. Adv.* **8**, eabg3827 (2022).
- Ebenig, A. et al. Vaccine-associated enhanced respiratory pathology in COVID-19 hamsters after TH2-biased immunization. *Cell Rep.* **40**, 111214 (2022).
- Zhang, T. et al. Th2 and Th17-associated immunopathology following SARS-CoV-2 breakthrough infection in Spike-vaccinated ACE2-humanized mice. *J. Med. Virol.* **96**, e29408 (2024).
- Wolfel, R. et al. Virological assessment of hospitalized patients with COVID-2019. *Nature* **581**, 465–469 (2020).
- Godiska, R. et al. Human macrophage-derived chemokine (MDC), a novel chemoattractant for monocytes, monocyte-derived dendritic cells, and natural killer cells. *J. Exp. Med.* **185**, 1595–1604 (1997).
- Imai, T. et al. Selective recruitment of CCR4-bearing Th2 cells toward antigen-presenting cells by the CC chemokines thymus and activation-regulated chemokine and macrophage-derived chemokine. *Int. Immunol.* **11**, 81–88 (1999).
- Polack, F. P., Hoffman, S. J., Crujeiras, G. & Griffin, D. E. A role for nonprotective complement-fixing antibodies with low avidity for measles virus in atypical measles. *Nat. Med.* **9**, 1209–1213 (2003).
- Heininger, U. et al. The concept of vaccination failure. *Vaccine* **30**, 1265–1268 (2012).
- Roberts, A. et al. Immunogenicity and protective efficacy in mice and hamsters of a beta-propiolactone inactivated whole virus SARS-CoV vaccine. *Viral Immunol.* **23**, 509–519 (2010).
- Handrejk, K. et al. Characterization of a SARS-CoV-2 Omicron BA.5 direct-contact transmission model in hamsters. *Npj Viruses* **2**, 52 (2024).
- Lindstrom, N. M., Moore, D. M., Zimmerman, K. & Smith, S. A. Hematologic assessment in pet rats, mice, hamsters, and gerbils:

- blood sample collection and blood cell identification. *Clin. Lab Med.* **35**, 629–640 (2015).
33. Fingerhut, L., Dolz, G. & de Buhr, N. What is the evolutionary fingerprint in neutrophil granulocytes? *Int. J. Mol. Sci.* **21**, <https://doi.org/10.3390/ijms21124523> (2020).
 34. Siegel, A. & Walton, R. M. Hematology and biochemistry of small mammals. *Ferrets Rabbits Rodents*, 569–582 <https://doi.org/10.1016/B978-0-323-48435-0.00039-3> (2020).
 35. Tomasi, V. H., Perez, M. A. & Itoiz, M. E. Modification of Luna's technique for staining eosinophils in the hamster cheek pouch. *Biotech. Histochem.* **83**, 147–151 (2008).
 36. Sekimukai, H. et al. Gold nanoparticle-adsorbed S protein induces a strong antigen-specific IgG response against severe acute respiratory syndrome-related coronavirus infection, but fails to induce protective antibodies and limit eosinophilic infiltration in lungs. *Microbiol. Immunol.* **64**, 33–51 (2020).
 37. Iwata-Yoshikawa, N. et al. Effects of Toll-like receptor stimulation on eosinophilic infiltration in lungs of BALB/c mice immunized with UV-inactivated severe acute respiratory syndrome-related coronavirus vaccine. *J. Virol.* **88**, 8597–8614 (2014).
 38. Nakayama, E. E. & Shioda, T. SARS-CoV-2 related antibody-dependent enhancement phenomena in vitro and in vivo. *Microorganisms* **11**, <https://doi.org/10.3390/microorganisms11041015> (2023).
 39. Li, D. et al. In vitro and in vivo functions of SARS-CoV-2 infection-enhancing and neutralizing antibodies. *Cell* **184**, 4203–4219.e4232 (2021).
 40. Bourmazos, S., Gupta, A. & Ravetch, J. V. The role of IgG Fc receptors in antibody-dependent enhancement. *Nat. Rev. Immunol.* **20**, 633–643 (2020).
 41. Schafer, A. et al. Antibody potency, effector function, and combinations in protection and therapy for SARS-CoV-2 infection in vivo. *J. Exp. Med.* **218**, <https://doi.org/10.1084/jem.20201993> (2021).
 42. Blue, C. E., Spiller, O. B. & Blackbourn, D. J. The relevance of complement to virus biology. *Virology* **319**, 176–184 (2004).
 43. Karwaciak, I., Salkowska, A., Karas, K., Dastych, J. & Ratajewski, M. Nucleocapsid and spike proteins of the coronavirus SARS-CoV-2 induce IL6 in monocytes and macrophages-potential implications for cytokine storm syndrome. *Vaccines* **9**, <https://doi.org/10.3390/vaccines9010054> (2021).
 44. Pan, P. et al. SARS-CoV-2 N protein promotes NLRP3 inflammasome activation to induce hyperinflammation. *Nat. Commun.* **12**, 4664 (2021).
 45. Nakayama, E. E. et al. Anti-nucleocapsid antibodies enhance the production of IL-6 induced by SARS-CoV-2 N protein. *Sci. Rep.* **12**, 8108 (2022).
 46. Batra, M. et al. Role of IgG against N-protein of SARS-CoV2 in COVID19 clinical outcomes. *Sci. Rep.* **11**, 3455 (2021).
 47. Nouailles, G. et al. Temporal omics analysis in Syrian hamsters unravel cellular effector responses to moderate COVID-19. *Nat. Commun.* **12**, 4869 (2021).
 48. Zhu, J. T helper 2 (Th2) cell differentiation, type 2 innate lymphoid cell (ILC2) development and regulation of interleukin-4 (IL-4) and IL-13 production. *Cytokine* **75**, 14–24 (2015).
 49. Boyce, T. G. et al. Lack of evidence for vaccine-associated enhanced disease from COVID-19 vaccines among adults in the vaccine safety datalink. *Pharmacoevid. Drug Saf.* **33**, e5863 (2024).
 50. Percie du Sert, N. et al. The ARRIVE guidelines 2.0: updated guidelines for reporting animal research. *PLoS Biol.* **18**, e3000410 (2020).
 51. Gerhards, N. M. et al. Predictive value of precision-cut lung slices for the susceptibility of three animal species for SARS-CoV-2 and validation in a refined hamster model. *Pathogens* **10**, <https://doi.org/10.3390/pathogens10070824> (2021).
 52. Corman, V. M. et al. Detection of 2019 novel coronavirus (2019-nCoV) by real-time RT-PCR. *Euro. Surveill.* **25**, 2000045 (2020).
 53. Pfaffl, M. W. A new mathematical model for relative quantification in real-time RT-PCR. *Nucleic Acids Res.* **29**, e45 (2001).
 54. Geiss, G. K. et al. Direct multiplexed measurement of gene expression with color-coded probe pairs. *Nat. Biotechnol.* **26**, 317–325 (2008).
 55. Metsalu, T. & Vilo, J. ClustVis: a web tool for visualizing clustering of multivariate data using principal component analysis and heatmap. *Nucleic Acids Res.* **43**, W566–W570 (2015).

Acknowledgements

We thank Berend Jan Bosch and Wentao Li (University of Utrecht, The Netherlands) for providing us with the anti-spike S1 antibody used in this study for staining of the cell monolayers in the virus neutralization assay. Illustrations in Fig. 1 were created with BioRender.com. We thank Stephen Gordon and John Browne (UCD Veterinary Sciences Centre, Dublin, Ireland) for performing the measurements on the nCounter®MAX Analysis System (NanoString Technologies, Seattle, WA, USA). We are grateful to all animal biotechnicians, laboratory and pathology colleagues at Wageningen Bio-veterinary Research for their excellent work, commitment, and support. We thank Amy C. Shurtleff, Trevor Brasel, Victoria Graham, William Dowling and Javier Castillo-Olivares from CEPI (Coalition for Epidemic Preparedness Innovations) for sharing ideas and expertise on study design and data interpretation. Finally, we would like to honor the memory of Robert D. Small, who was instrumental in designing and statistical analysis of the experiments included in this work. His inspirational attitude and ingenious insights into the use of statistics for (pre) clinical study designs are greatly missed. This research was funded by the Coalition for Epidemic Preparedness Innovations (CEPI).

Author contributions

R.d.J. performed the two experiments, N.O., S.V., R.d.J., K.W., F.J.S. wrote the main manuscript, R.d.S. critically reviewed the manuscript, K.B. and Y.H. prepared and characterized the experimental vaccine preparation, N.O., R.d.J. and N.G. designed the experiment, J.L.G. performed the statistical analysis, N.O., R.d.J., S.V., J.S., M.C. K.W., F.J.S. and R.d.S. analyzed the data, all authors participated in data interpretation, and have read, edited and approved the submitted version of the manuscript.

Competing interests

The authors declare no competing interests.

Additional information

Supplementary information The online version contains supplementary material available at <https://doi.org/10.1038/s41541-025-01160-7>.

Correspondence and requests for materials should be addressed to Rineke de Jong or Nadia Oreshkova.

Reprints and permissions information is available at <http://www.nature.com/reprints>

Publisher's note Springer Nature remains neutral with regard to jurisdictional claims in published maps and institutional affiliations.

Open Access This article is licensed under a Creative Commons Attribution-NonCommercial-NoDerivatives 4.0 International License, which permits any non-commercial use, sharing, distribution and reproduction in any medium or format, as long as you give appropriate credit to the original author(s) and the source, provide a link to the Creative Commons licence, and indicate if you modified the licensed material. You do not have permission under this licence to share adapted material derived from this article or parts of it. The images or other third party material in this article are included in the article's Creative Commons licence, unless indicated otherwise in a credit line to the material. If material is not included in the article's Creative Commons licence and your intended use is not permitted by statutory regulation or exceeds the permitted use, you will need to obtain permission directly from the copyright holder. To view a copy of this licence, visit <http://creativecommons.org/licenses/by-nc-nd/4.0/>.

© The Author(s) 2025